

RESEARCH ARTICLE

Unveiling functional motions based on point mutations in biased signaling systems: A normal mode study on nerve growth factor bound to TrkA

Pedro Túlio Resende-Lara^{1,2}, David Perahia², Ana Lígia Scott¹, Antônio Sérgio Kimus Braz^{1*}

1 Laboratório de Biologia Computacional e Bioinformática, Universidade Federal do ABC, Santo André, São Paulo, Brazil, **2** Laboratoire de Biologie et Pharmacologie Appliquée, École Normale Supérieure Paris-Saclay, Cachan, Île-de-France, France

* antonio.braz@ufabc.edu.br



OPEN ACCESS

Citation: Resende-Lara PT, Perahia D, Scott AL, Braz ASK (2020) Unveiling functional motions based on point mutations in biased signaling systems: A normal mode study on nerve growth factor bound to TrkA. PLoS ONE 15(6): e0231542. <https://doi.org/10.1371/journal.pone.0231542>

Editor: Claudio M. Soares, Universidade Nova de Lisboa Instituto de Tecnologia Química e Biológica, PORTUGAL

Received: July 31, 2019

Accepted: March 26, 2020

Published: June 4, 2020

Copyright: © 2020 Resende-Lara et al. This is an open access article distributed under the terms of the [Creative Commons Attribution License](https://creativecommons.org/licenses/by/4.0/), which permits unrestricted use, distribution, and reproduction in any medium, provided the original author and source are credited.

Data Availability Statement: All relevant data are within the manuscript and its Supporting Information files.

Funding: This work was performed using HPC resources from the “Mésocentre” computing center of Centrale Supélec and École Normale Supérieure Paris-Saclay supported by Centre Nationale de Recherche Scientifique (CNRS, France) and Région Île-de-France (<http://mesocentre.centralesupelec.fr/>). We gratefully

Abstract

Many receptors elicit signal transduction by activating multiple intracellular pathways. This transduction can be triggered by a non-specific ligand, which simultaneously activates all the signaling pathways of the receptors. However, the binding of one biased ligand preferentially trigger one pathway over another, in a process called biased signaling. The identification the functional motions related to each of these distinct pathways has a direct impact on the development of new effective and specific drugs. We show here how to detect specific functional motions by considering the case of the NGF/TrkA-Ig2 complex. NGF-mediated TrkA receptor activation is dependent on specific structural motions that trigger the neuronal growth, development, and survival of neurons in nervous system. The R221W mutation in the *ngf* gene impairs nociceptive signaling. We discuss how the large-scale structural effects of this mutation lead to the suppression of collective motions necessary to induce TrkA activation of nociceptive signaling. Our results suggest that subtle changes in the NGF interaction network due to the point mutation are sufficient to inhibit the motions of TrkA receptors putatively linked to nociception. The methodological approach presented in this article, based jointly on the normal mode analysis and the experimentally observed functional alterations due to point mutations provides an essential tool to reveal the structural changes and motions linked to the disease, which in turn could be necessary for a drug design study.

Introduction

There is a plethora of protein receptors in nature responsible for eliciting different cellular responses by engaging distinct intracellular signaling cascades. Biased agonism, or functional selectivity, is the preferential activation of a receptor’s particular signal transduction pathway over another produced by the binding of a specific ligand. The suggested molecular mechanism of biased signaling is that a biased ligand stabilizes the receptor in the most favorable

acknowledge financial support from Universidade Federal do ABC (UFABC) and Coordenação de Aperfeiçoamento de Pessoal de Nível Superior (CAPES), process number: 88881.133141/2016-01 to PTRL.

Competing interests: The authors have declared that no competing interests exist.

conformation to interact with a given intracellular partner, which interaction triggers a specific signaling pathway [1–3]. The receptor's stabilization by the ligand can occur either on the orthosteric or the allosteric binding sites. Although, this phenomenon has been widely studied for G-protein coupled receptors [4–7], other receptor classes also exhibit such behavior, such as tyrosine kinase receptors [8,9].

Proteins adopt a multitude of conformations in solution, therefore their functions are intimately related to their structure and shape, and ultimately to their dynamics [10]. As mentioned above, the interaction with a ligand stabilizes one receptor's conformation over a large conformational set in equilibrium, shifting the equilibrium towards the bound form [11,12]. Hence, this shift is an effect of favoring certain protein's movements by the ligand. Let us consider a given multisignaling receptor that is able to elicit two different signal transduction pathways, α and β . The binding of a nonspecific ligand to it allows the complex to perform motions related to both signaling paths. Nonetheless, the complex with a biased ligand can activate only one of these pathways. Furthermore, a mutation in the receptor also may result in biased signaling (Fig 1). Although protein function is related to specific motions, much of the protein dynamics is not linked to any functional role. These nonfunctional motions are also illustrated in Fig 1.

Is it possible to identify the motions related to different transduction pathways of a multisignaling receptor? What are the molecular mechanisms involved in each signaling pathway? The answers to these questions may provide some insight into how conformational changes

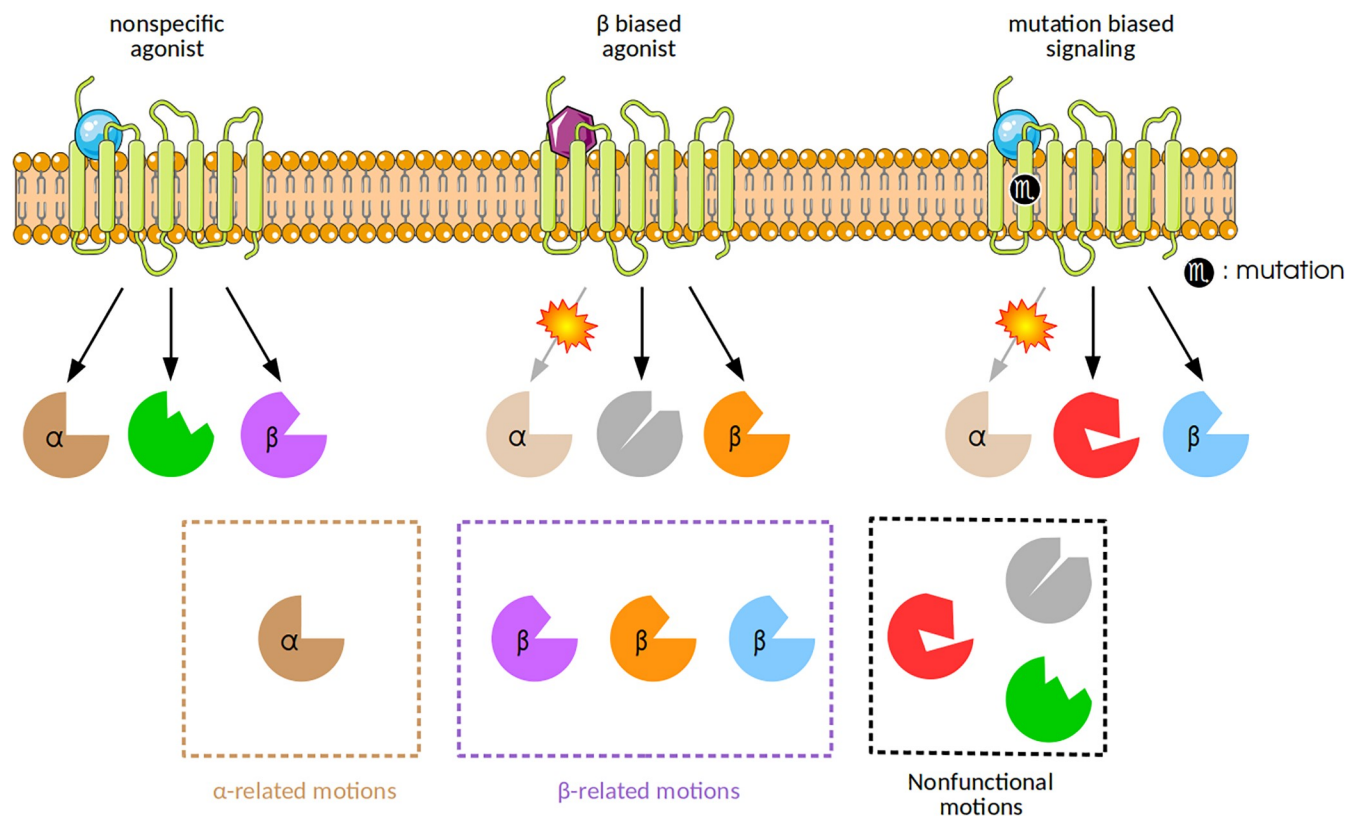


Fig 1. Multisignaling receptors and biased signaling. The binding of a nonspecific ligand (blue sphere) to a multisignaling receptor promotes a change in the receptor's dynamics. This change results in motions that are linked to α and β signaling pathways (brown and purple shapes, respectively). On the other hand, a biased ligand (purple hexagon) is able to activate a singular signaling path (β , orange shape). A mutation in the receptor can also result in biased signaling. In this figure, the interaction of a nonspecific ligand with the mutant receptor results in the activation of β signaling path (blue shapes), but not the α one. In addition, the presence of nonfunctional motions are observed in all interactions.

<https://doi.org/10.1371/journal.pone.0231542.g001>

trigger distinct intracellular responses. This has a direct impact on the understanding of pathological conditions as well as on the development of new specific and efficient drugs. In this work, we address these questions using the NGF/TrkA complex as a case study. We describe functional motions presented by NGF/TrkA-Ig2 wild type complex as the trigger to nociceptive signaling. We show that the R221W mutation of NGF irreversibly remove these motions. Widespread structural changes such as flexibility, hydrogen bonds, salt bridges and substructure dynamic coupling rearrangements differ between wild type neurotrophic- and nociceptive-related motions as well as for mutant structures.

The tropomyosin-related receptor kinase type A (TrkA) is related to growth, differentiation and survival of cholinergic, sympathetic and sensory neurons in both central and peripheral nervous systems. TrkA is found as inactive non-covalently associated dimers in neurite membrane [13] and its signaling is activated by the high affinity interaction with nerve growth factor (NGF) [14]. Each TrkA monomer is composed of (from outside to inside): two cysteine-rich motifs (CR) interrupted by a leucine-rich repetition domain (LRR), two immunoglobulin-like domain (Ig), a transmembrane helix and an intracellular tyrosine kinase domain (Fig 2A).

The interface between NGF and TrkA receptors occurs mainly in two sites (Fig 2B): i) the specific patch, composed by residues of NGF N- and C-terminal portions and TrkA AB sheet (Fig 2C); and ii) the conserved patch, between TrkA EF loop and NGF β -sheets (Fig 2D). In addition, NGF loops L1, L2 and L4 are proposed to interact with the linker between Ig2 domain and the membrane [15]. Functional assays have described the importance of several residues along these regions in binding and specificity [16–24]. Although many of them are located in interface regions, residues in NGF loop L3 and TrkA-Ig2 CFG β -strands also play a role in binding and/or specificity. Specific patch interactions are thought to govern the specificity of NGF binding to TrkA and conserved patch has this name because residues in this region are highly conserved in NGF and TrkA families.

NGF promotes conformational changes in TrkA resulting in the trans-autophosphorylation of a set of intracellular tyrosines. It is well known that the interactions between TrkA and NGF occurs mainly in Ig2 domain [25]. The deletion of this domain turned TrkA receptors constitutively active in the absence of NGF [26] while the whole receptor is inactive by itself. Therefore, it is the NGF/TrkA-Ig2 domain interaction that induces the activation of the cell response resulting in neuronal growth and differentiation. Although the cysteine and leucine-rich sequences are not required for neuronal proliferation, they are important for fully differentiation activity [26,27]. Nevertheless, the whole TrkA dimer undergoes a dynamical change induced by the NGF/TrkA-Ig2 interaction and resulting motions. These motions are supposed to be the rotation of TrkA dimer as described for other receptors tyrosine kinases (RTKs) like ErbB family members [28–31]. In the TrkA tyrosine kinase domain, phosphorylation of Y496 regulates neuronal differentiation and cell survival, while phosphorylation of Y791 induces gene expression and cell differentiation [32] (left panel–Fig 3).

Individuals with Hereditary Sensory and Autonomic Neuropathy Type 5 (HSAN5) has impaired sensitivity of pain, heat or cold. HSAN5 is caused by a single mutation in the *ngf* gene, replacing an arginine by a tryptophan at position 221 (R221W). There is no other damage in sensory fibers type C unless the failure in NGF/TrkA signaling [33,34]. The neurotrophic activity of R221W mutant is not compromised [35]. The deep pain, i.e., pain related to muscle, bone, and ligaments is especially affected in this pathology, being common cases of repeated bone and joints traumas that evolve to neurogenic arthropathy due the loss of sensitivity of pain [34–36] (right panel–Fig 3).

As described, phosphorylation of TrkA residue Y496 recruits pro-survival PI3K/AKT pathway while Y791 recruits pro-differentiation PLC γ 1 pathway. The R221W mutant is capable to induce the PI3K/AKT pathway, responsible to neuronal survival, however, PLC γ 1 pathway is

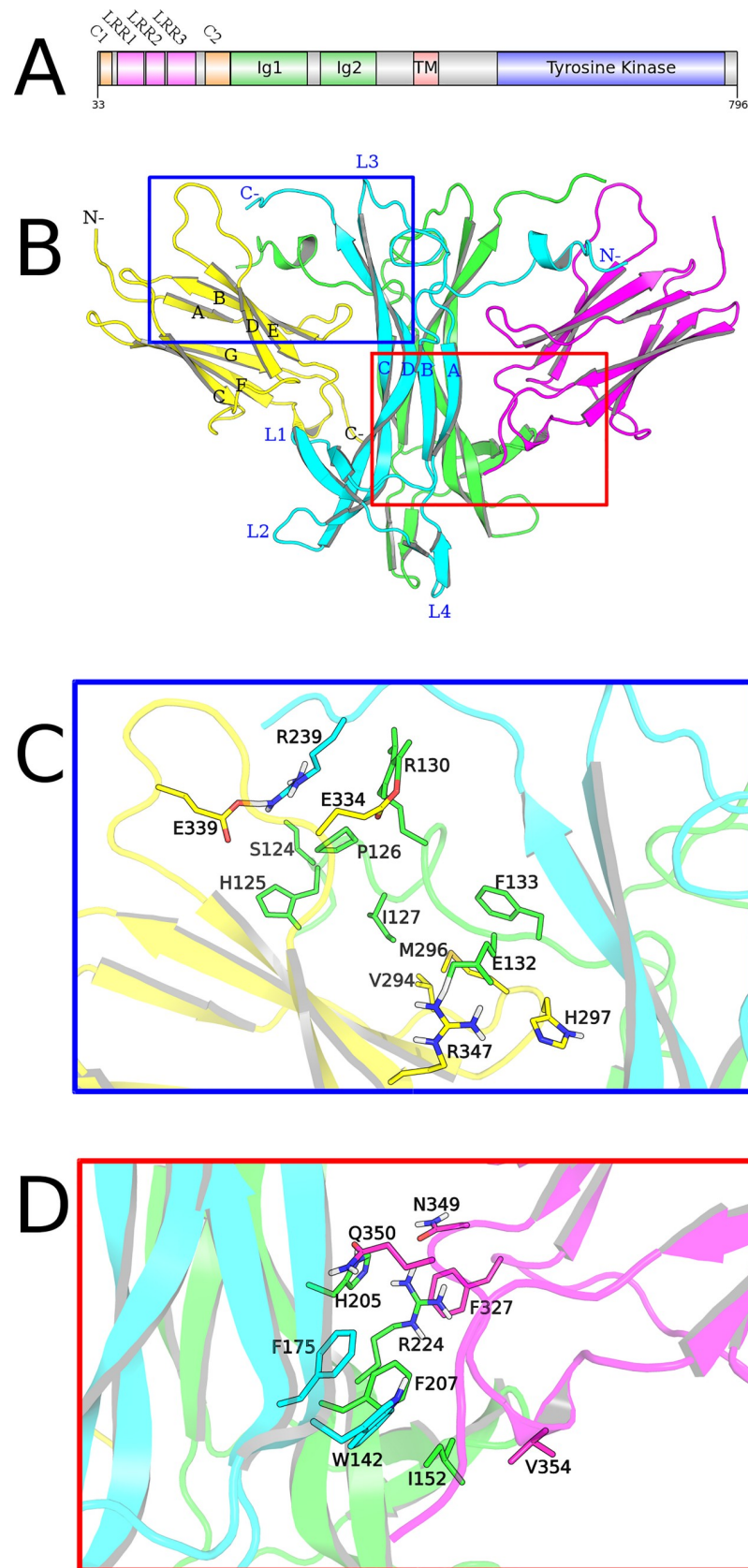


Fig 2. NGF/TrkA-Ig2 complex and binding sites. (A) Domain organization of TrkA. Domains are colored in: orange, cysteine-rich clusters (C1-2); in magenta, leucine-rich repetitions (LRR1-3); in green, immunoglobulin-like domains

(Ig1-2); in red, transmembrane portion (TM); and in blue, tyrosine kinase domain. (B) NGF/TrkA-Ig2 complex motif description. (C) Specific and (D) conserved NGF/TrkA epitopes. Chains are colored as: NGF_A: green; NGF_B: cyan; TrkA_A: magenta; TrkA_B: yellow.

<https://doi.org/10.1371/journal.pone.0231542.g002>

not induced [35]. The biological mechanism of HSAN5 has been discussed in the literature [33,34,37,38]. The diminished secretion of mature NGF and/or a reduced activation of specific intracellular pathways stand out among the hypotheses raised.

Results

R221W mutant loses functional motions and introduce new non-functional ones

TrkA has a biased signaling, promoting neuroprotective properties and nociceptive innervation in sensory neurons. Due to this signaling nature, it is expected at least two sorts of

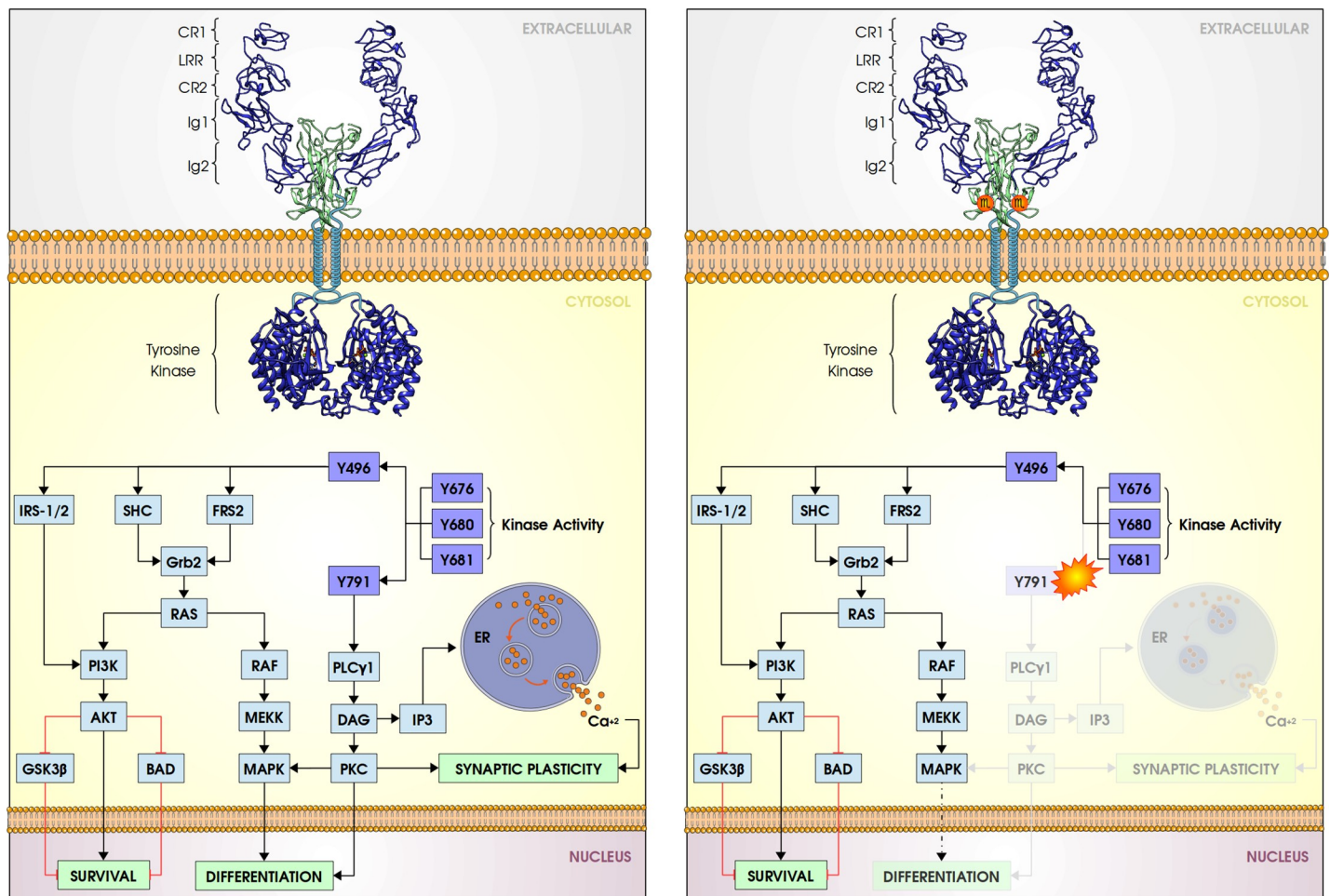


Fig 3. TrkA intracellular signaling activated by wild type and mutant NGF. (Left panel) Wild type signaling. NGF (green cartoon) promotes TrkA (blue cartoon) signaling mediated by phosphorylation of intracellular tyrosine residues (dark blue boxes). Phosphorylated Y496 forms an adaptor binding site that couple mitogen-activated protein kinases (MAPKs) and phosphoinositide 3-kinase (PI3K) signaling pathways, activating transcription of genes related to neuronal differentiation and survival, respectively. Phosphorylation of Y791 activates phospholipase C γ 1 (PLC γ 1) pathway, that mediates neuronal differentiation and synaptic plasticity via PKC and Ca²⁺ cytosolic release, respectively. Autophosphorylation of residues Y676, Y680 and Y681 mediates TrkA kinase activity and modulates Y496 and Y791 signaling. (Right panel) R221W mutant signaling. R221W mutation (orange spheres in NGF cartoon) incapacitates the induction of Y791 signaling pathway, impairing neuronal differentiation and synaptic plasticity, that results in the insensitivity to pain, heat and cold in HSAN5.

<https://doi.org/10.1371/journal.pone.0231542.g003>

motions governing NGF/TrkA signaling: one promoting neurotrophic response (Q_{NTR}), that is present in both wild type and mutant; and another promoting nociceptive perception (Q_{NCP}), that is absent with R221W mutation. To characterize the functional motions involved in each NGF/TrkA complex signaling outcome, we performed a mass-weighted displacement along the 20 lowest frequency normal modes to obtain relaxed pseudo-trajectories along these modes. This allows us to obtain the minimum energy pathway under the normal mode restraint potential, favoring the system to go beyond the harmonic approximation inherent to NMA. Then, we evaluated the similarities between these pseudo-trajectories according to the Mantel test (see details in [Methods](#)). Briefly, this procedure consists in computing the relative displacement related to each pseudo-trajectory and compare them to each other. The pseudo-trajectories that are similar to each other are considered to present closely related motions and, therefore, were clustered together. We preferred this approach to directly comparing normal mode vectors between them since we better take into account of the anharmonic effects, and furthermore we can compare structural deviations of specific regions.

We found a motion that describes the torsion of the NGF dimer coupled to a rotation of TrkA-Ig2 monomers perpendicular to the NGF motion ([Fig 4A and 4B](#)), similar to what has been observed previously by Settanni and colleagues with a principal component analysis of molecular dynamics simulations [39]. Mantel similarity scores of C α atomic displacements showed that this motion is preserved in a number of WT and R221W normal modes (red and green circles in [Fig 5](#), respectively). Thus, since both wild type and mutant structures present this above described type of motion, we hypothesized that it corresponds to the motion responsible for inducing the trophic response of TrkA (Q_{NTR}).

Nonetheless, seven WT modes were totally independent (blue circles in [Fig 5](#)), showing no significant similarity of C α atomic displacements with any other motions whether in WT or R221W. The existence of some WT isolated modes is in agreement with the idea of the presence of a Q_{NCP} motion responsible for triggering the TrkA nociceptive signaling pathway. In addition, we noticed ten modes in R221W mutant structure that showed no significant Mantel similarity score either between other mutant motions or WT ones (magenta circles in [Fig 5](#)). This means that, besides the absence of Q_{NCP} motions, these mutant non-functional motions (Q_{MUT}) may or may not have functional significance, which it is not possible to assert by our method. Detailed similarity data are available in [S1 Table](#).

We then investigated if R221W structure could reproduce the Q_{NCP} motions trajectories. Hence we applied the wild type Q_{NCP} motions to the R221W structure and generated relaxed structures along these directions, which was called hQ_{NCP} . Mantel comparison tests between hQ_{NCP} and Q_{NCP} motions showed that R221W mutant does not fully reproduce the WT Q_{NCP} motions. Only 2 out of 7 motions were preserved by the mutant structure ([S2 Table](#)) indicating clearly that the mutation interferes importantly with the global motions.

We performed additional mutations at 221 position to ensure the role of contacts change in the loss of nociceptive-related motions. The R221E mutation, known to possess the same features that R221W [34], presented a similar motion correlation pattern to R221W, also losing non-trivial modes 07, 09, 16, 20 and 24 ([S3 Table](#)). When changing the arginine to an alanine, the results were even more drastic: beyond the loss of all nociceptive-related motions, a massive decrease in correlated neurotrophic-related ones was observed, losing the redundancy presented by WT structure ([S3 Table](#)). Changing R221 to a lysine, although maintaining similar electrostatic features, did not lead to recover the WT motion correlation profile. Taken together, these results draw a picture of how local topological changes lead to large collective distortions, regardless the size or charge of the mutant side-chains.

In order to evaluate the sensitivity of this protocol, we analyzed mutations that are rather or not related to pathogenic effects occurring both at NGF and TrkA structures. NGF mutation F133L is a

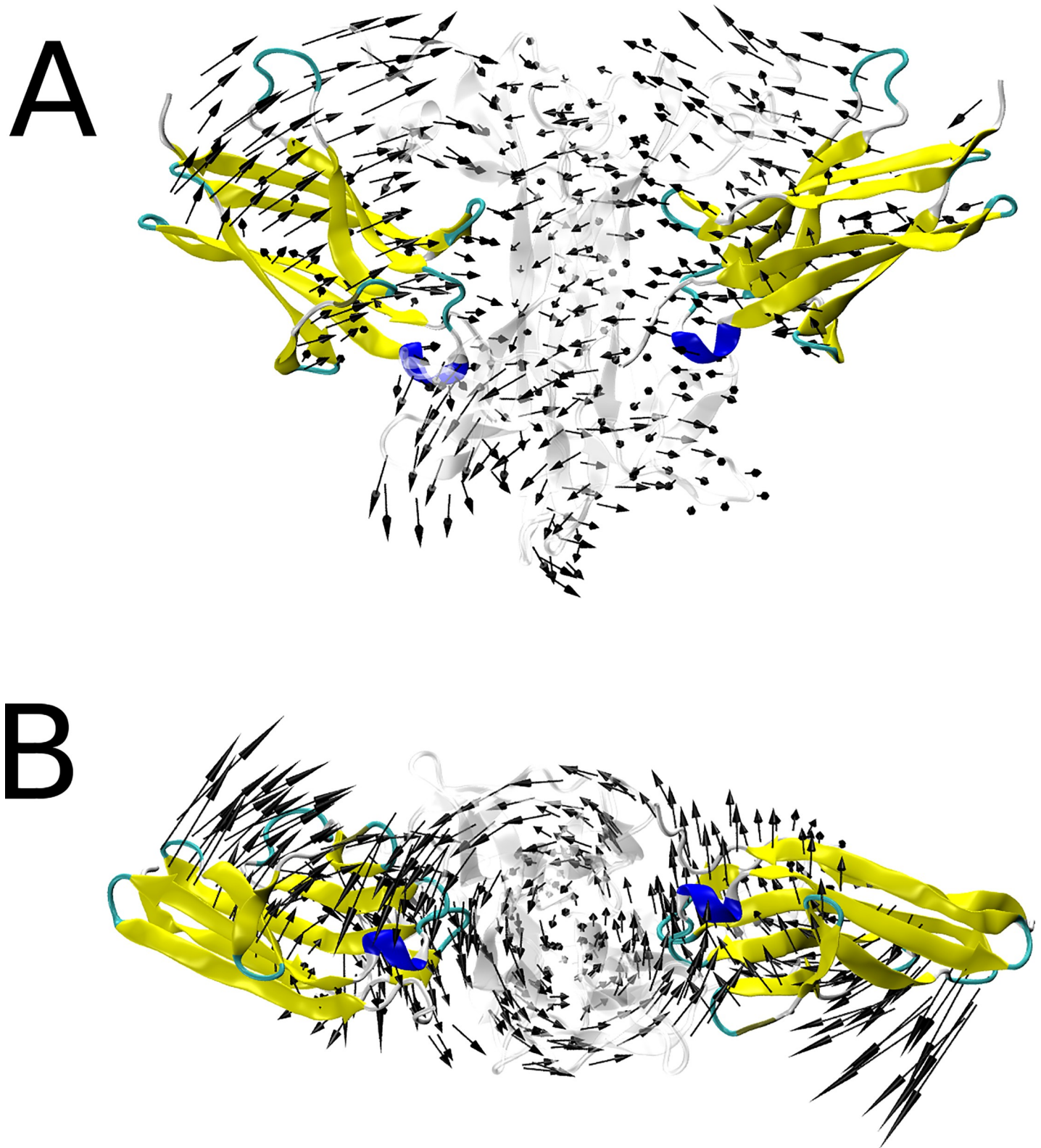


Fig 4. Representation of neurotrophic and nociceptive related motions. (A) Frontal and (B) bottom view of WT mode 11, that show NGF torsional motions approaching TrkA-Ig2 subunits. NGF dimer is represented in transparent cartoon, and TrkA is represented by secondary structure colored cartoon. Black arrows are normal mode eigenvectors placed at C α atoms.

<https://doi.org/10.1371/journal.pone.0231542.g004>

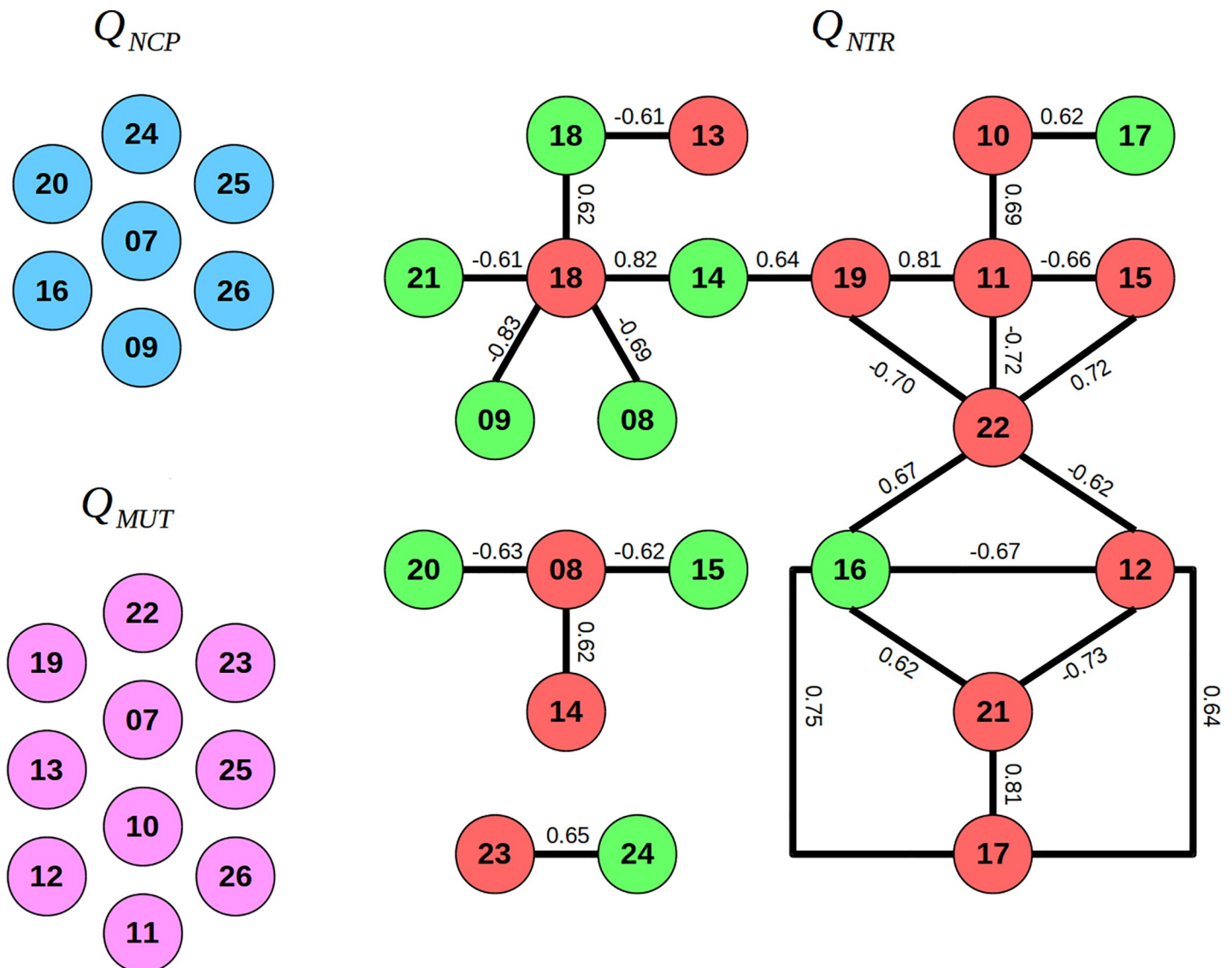


Fig 5. Motion redundancy among the 20 lowest frequency normal modes computed for TrkA complexed with wild type and mutant NGF. The mantel similarity scores revealed that a number of WT and R221W normal modes (red and green nodes, respectively) preserve a given motion. Thus, since both WT and mutant NGF are capable to induce neurotrophic response, these similar modes are putatively assigned to activate the neurotrophic bias of TrkA. On the other hand, independent WT motions (blue nodes), that have no similarity either with all other WT motions or R221W ones, are hypothesized as responsible for nociceptive bias of TrkA, since they are present only in WT structures. Also, independent R221W motions (magenta nodes) may introduce an impairment in communication pathways. Numbers in circles are non-trivial NM numbers of respective systems. Values on edges correspond to the Mantel similarity scores between the connected modes; only pairs of modes with similarity score greater than $|0.6|$ were connected in these graphs. Note that the modes considered start with the number 7, since the modes from 1 to 6 correspond to trivial overall translation/rotation of the system.

<https://doi.org/10.1371/journal.pone.0231542.g005>

potentially deleterious mutation found in HSAN5; and TrkA mutation Y359C was found in Congenital Insensitivity to Pain with Anhidrosis (CIPA). Both diseases present loss of nociceptive activity of NGF/TrkA complex, while HSAN5 has milder effects compared to CIPA. Mutations V185I (NGF) and R314V (TrkA) do not present deleterious effects on the intracellular signaling.

We observed that F133L did not reproduce nociceptive-related motions (excepting WT motion 07). Interestingly, F133 residue is located at the NGF/TrkA interface and has, therefore, a role at the complex interaction. Oppositely, TrkA residue Y359 is located inside the TrkA Ig2 domain and has no direct contact with NGF. Nonetheless, Y359C mutant do not

activate the nociceptive signaling pathway, causing partial loss of function and a less severe deficiency of unmyelinated axons but a greater effect on small myelinated fibers [40]. Our results showed that the putative nociceptive-related motions were lost also in this mutant. Moreover, it presented an increased number of mutant motions compared to the other structures. This is an interesting observation since the biological impairment of this mutant are more severe than the previous ones. Regarding the silent mutants, both neurotrophic- and nociceptive-related motions are shown highly correlated (S3 Table). In summary, these data present strong evidence of the robustness of this protocol to identify functional motions in biased signaling systems.

Structural cross-correlation: Large differences between functional and non-functional motions

The signal transmission within protein complexes usually arises from a coupling of motions between allosteric or interface regions [41–43]. These regions are the basis of communication between proteins and, therefore, are expected to move in a coordinated fashion. In order to characterize the collective character of WT and R221W motions, the structural cross-correlation matrix ($C_{(i,j)}$) of $C\alpha$ atoms of each motion within the clusters were calculated.

A general pattern was observed in which the NGF subunits are highly correlated with each other, indicating that they move in a coordinated fashion to bind TrkA in any type of motion (Fig 6). This is in agreement with experimental data showing that wild type and mutant NGF binds to TrkA with similar affinity [38]. As expected, the Q_{NTR} motions of the WT and R221W structures show a very similar residue cross-correlation profile (Fig 6A and 6C). The similarity between the observed residue coupling patterns is in agreement with the evidence of biased character of TrkA signaling [8,44], supporting the idea that these preserved motions are those responsible to inducing neurotrophic and neuroprotective signaling pathways. Remarkably, TrkA_B residues A364, F367, Q369 and S371 are strongly anti-correlated with NGF_B AB and CD β -strands residues in mutant and wild type Q_{NTR} motions, respectively (black rectangles in Fig 6A and 6C). These residues are located far from the interface regions but are linked to NGF_B residues, and are shown to play a role in TrkA activation (H205, F207 and R224).

Q_{NCP} motions have the highest number of highly correlated and anti-correlated residue pairs in the entire complex (Fig 6B). The NGF chains present even more residues with moderate and strong couplings between them than in Q_{NTR} motions. In particular, it is observed that the TrkA subunits are moderately coupled (green square in Fig 6B). Nonetheless, NGF and TrkA present more anti-correlated residues with moderate or strong couplings than in Q_{NTR} . Main interactions occur between TrkA_A AB EFG β -strands and NGF N-terminal region and CD β -strands on both chains (black rectangle in Fig 6B). In addition, there are residues coupled in CD loop of TrkA_B and NGF_B C-terminal region. Together, these differences in dynamic couplings could indicate that the NGF and TrkA chains move in a more coordinated way in Q_{NCP} than in Q_{NTR} motions. The Q_{MUT} motions generally show a decrease in the number of moderately and strongly coupled residues throughout the complex (Fig 6D). Remarkably, we observed the absence of moderate or strong coupling between the TrkA chains, demonstrating that they do not move in a coordinated manner. In other words, in addition to the loss of Q_{NCP} motions, the inability to establish long range couplings between the distal residues may be a cause of the dysfunctional behavior of mutant NGF.

Dynamical network: Biological function is related to fewer structural partitions

To further dissect the dynamic couplings, dynamical correlation networks were constructed in which the nodes represent the $C\alpha$ protein atoms, and edges are weighted by their correlation

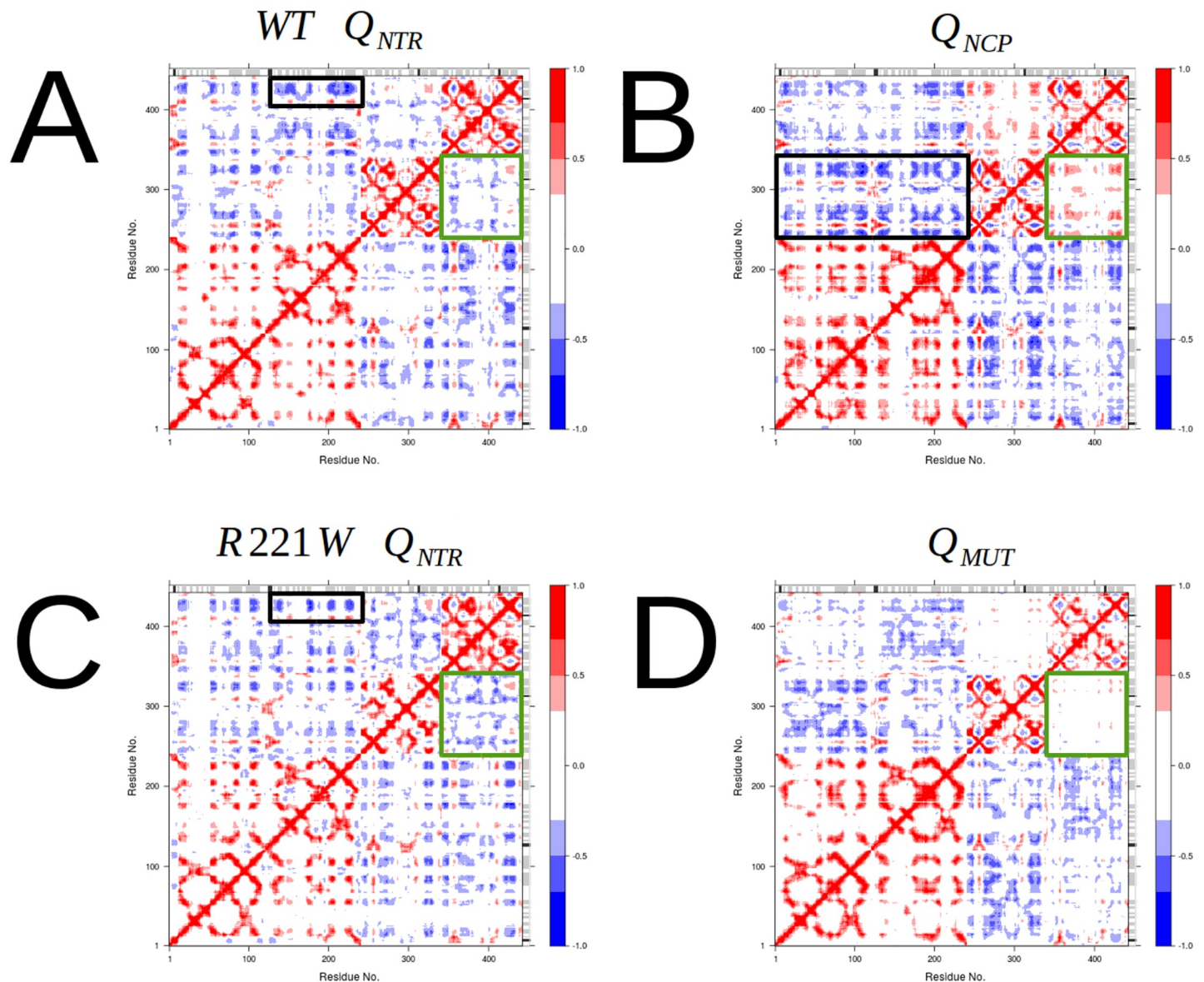


Fig 6. Dynamic Cross-Correlation Map (DCCM) of atomic displacements for all residue pairs in different types of motions. (A) DCCM of WT Q_{NTR} motions. TrkA chains show moderate anti-correlation between them (green square). The NGF_B and TrkA_B chains have strongly anti-correlated residues (black rectangle). (B) DCCM of Q_{NCP} motions. TrkA chains show a more consistent moderate correlation with each other (green square), indicating that they move in a coordinate fashion in the same direction. The same was observed for NGF. Also, more strongly anti-correlated residues were observed involving all chains (black rectangle). (C) The DCCM of the R221W Q_{NTR} motions have a very similar pattern to that of the WT Q_{NTR} . (D) The DCCM of the Q_{MUT} motions. Residue pair correlations are weaker throughout the structure in these motions. TrkA chains are uncoordinated (green square).

<https://doi.org/10.1371/journal.pone.0231542.g006>

values. Then, a hierarchical clustering of edges is used to determine the local communities of highly correlated residues, which constitute partitioned substructures within which the residues are strongly intra-connected, but are weakly inter-connected with those of other regions (see [Methods](#) for details). Nodes in the same community can easily communicate with each other. In contrast, nodes involved in inter-community communication are rarer and have been shown to be more critical for protein signaling [45–48].

A general community composition is shared by all type of motions. NGF is mostly broken down into three communities: the first is formed by the regions of the β -sheet bundle, the

cystine-knot, and the L3 loop of the two chains (blue in Fig 7). The second and third include L1, L2, and L4 loops of NGF_A and NGF_B, respectively (red and yellow in Fig 7, respectively). Each TrkA subunit is dynamically partitioned into a single community, which also includes the N-terminal part of NGF at the specific patch interface (orange for TrkA_A and silver for TrkA_B in Fig 7, respectively).

Despite their similarities in the dynamic coupling, the Q_{NTR} networks reveal interesting differences when the WT and R221W motions are taken into account separately (Fig 7A and 7B). The main difference is that the mutant structure has a partition of N- and C-terminal regions of NGF_A and NGF_B, respectively, constituting a new small community (green, Fig 7B) apart from the large community formed by NGF β -sheet bundle and loop L3 of the two chains (blue). The R221W Q_{NTR} network also differs by loosening the communication between the L2 loops of NGF chains, once in direct contact with the WT Q_{NTR} network.

Q_{NCP} motions present the least partitioned network (Fig 7C). There is a fusion of the β -sheet bundle community and those formed by loops L1, L2, and L4 of NGF_A. Another difference compared to Q_{NTR} lies on the lack of coupling between the L2 loops of the NGF chains. However, the two WT networks exhibit a similar coupling between the NGF and TrkA subunits, while the mutant exhibits an asymmetric binding profile between NGF and TrkA.

Regarding the communication between NGF and TrkA residues, an interesting set of couplings stand out. Q_{NTR} motions exhibit M296 and H297 of the two TrkA chains as principal coupled residues by the N-terminal part of NGF. These residues are part of a specific patch interface, and this pattern was also found in the Q_{NCP} and Q_{MUT} motions. Interestingly, the Q_{NTR} network of the two WT and R221W structures present the H205 (NGF_B) and Q350 (TrkA_B) residues dynamically coupled (magenta circles in Fig 7A and 7B). The same was not observed for the Q_{NCP} and Q_{MUT} motions. This coupling occurs at the conserved patch interface, in which there are many conserved residues within the NGF and TrkA families. This suggests that different signaling outcomes are activated by changing the dynamic coupling of both binding sites, highlighting the importance of structural communication in biological response. Also, the coupling of loops L1, L2, and L4 of each NGF chain into the same community highlights the role played by these regions in signaling. Since they are thought to interact with the TrkA linker next to the transmembrane helix [15], the rotational motions presented by these loops can help promote the conformational change necessary for functional signaling.

Optimal and suboptimal paths: Different couplings of interface residues in Q_{NTR} and Q_{NCP} motions

Betweenness centrality is a measure of the influence of a node on the information flow in dynamical networks. It is defined as the number of shortest paths between pairs of other nodes that run through a node [49]. Assuming that information flows more efficiently through the shortest paths, a node connecting the communities will have a high centrality. This property allows us to quantify the relative importance of each residue in the correlated motions.

Interface residues present the highest centrality values in all networks (Fig 8), reinforcing the expected importance of these residues for the communication in the complex. Q_{NTR} motions show high centrality values at both specific and conserved patch residues: H297 of TrkA_A and Q350 of TrkA_B (Fig 8A). On the other hand, only residues of specific patch have high centrality values in Q_{NCP} and Q_{MUT} motions (H297 of both TrkA chains) (Fig 8B). This indicates that network communities are linked differently depending on the motion, recruiting different binding site residues to induce each signaling outcome. Surprisingly, the main difference between Q_{NCP} and Q_{MUT} motions is the great increase in F133 centrality in both NGF chains observed in Q_{MUT} motions. This residue is located in the N-terminal region, 37 Å far

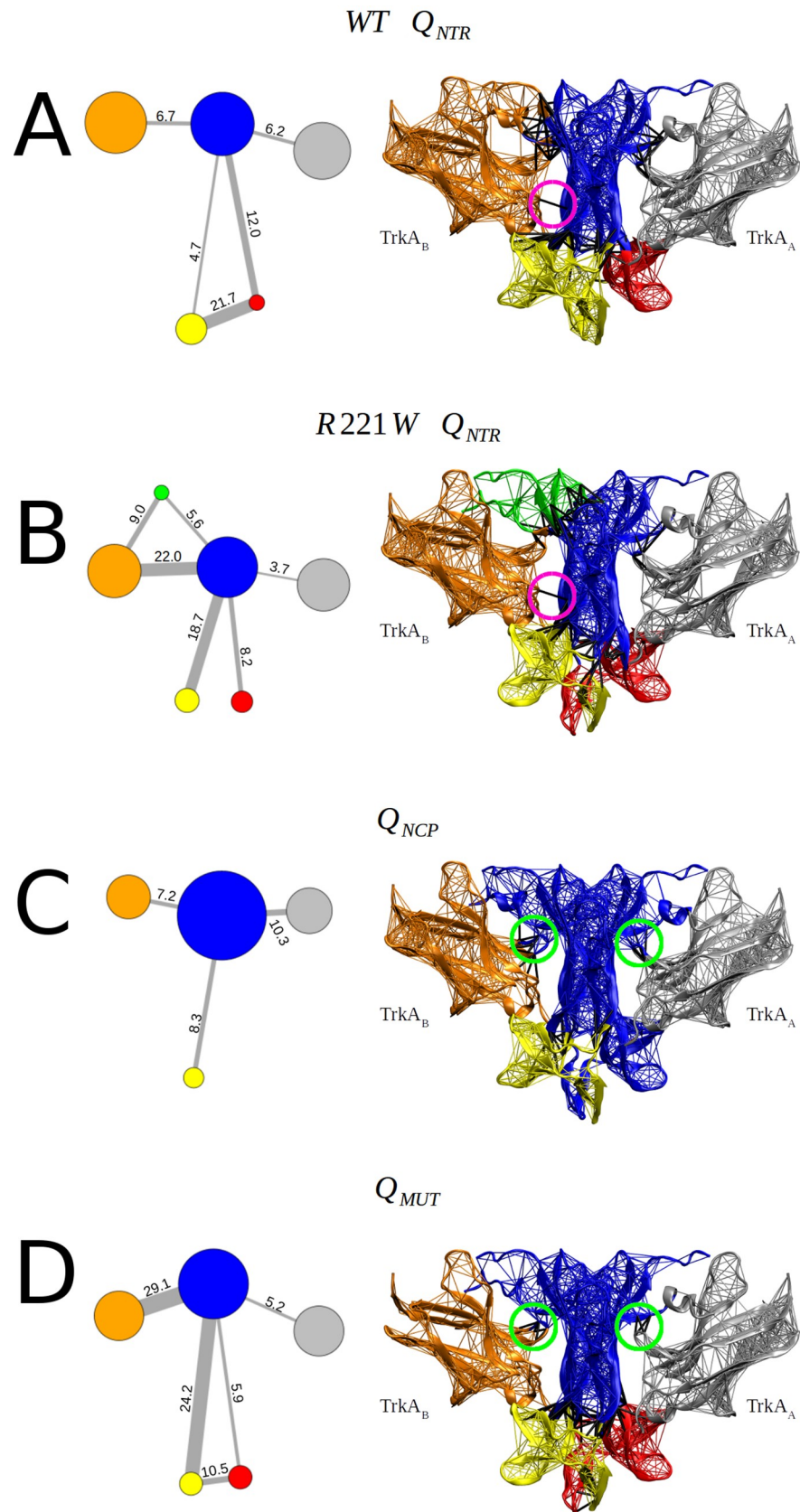


Fig 7. Community analysis reveals differences in the dynamic coupling of the complex. Mapping of the molecular structure of network communities (colored regions) and residue couplings (lines) of (A) WT Q_{NTR} , (B) R221W Q_{NTR} , (C) Q_{NCP} , and (D) Q_{MUT} . Q_{NTR} motions shows the coupling of communities in specific and conserved binding sites. In particular, in the two WT networks, the NGF main community (blue) links TrkA subunits with a similar strength while those in the mutants exhibit asymmetric behavior, coupling TrkA_B with much more strength than TrkA_A. Left panel: the relative radius of circles indicates the number of residues in a particular community. The values on the edges correspond to the relative strength of inter-community coupling. Right panel: the magenta circles highlight the dynamic coupling of residues H205 (NGF_B) and Q350 (TrkA_B), and the green circles indicate the coupling of F133 (NGF) and H297 (TrkA) in the two chains. Inter-community couplings are indicated with black lines.

<https://doi.org/10.1371/journal.pone.0231542.g007>

from the mutation, connecting the main NGF community and the TrkA communities, including residue H297 (green circles in Fig 7C and 7D).

The distinct involvement of each binding site with motions related to neuroprotective or nociceptive signaling was further characterized by the calculation of optimal and suboptimal paths between residues in interface regions of both TrkA chains. This approach consists to calculate 500 suboptimal connecting paths between a selected pair of residues, describing the alternative paths of dynamic communication flow among them [45]. The correlations between the residues along the path in the network—and as a consequence, the complex allosteric signaling—increase as the path length decreases, the latter being defined as the sum of the respective edge weights crossed [46].

Suboptimal path analysis revealed a shorter overall communication between conserved patch residues in Q_{NTR} than in Q_{NCP} motions. Concerning the specific patch, an interesting difference can be noticed: residues with high centrality in TrkA AB loop are connected by shorter paths in Q_{NTR} motions, while suboptimal paths between residues with lower centrality in DE loop are longer in these motions than in Q_{NTR} . In almost all cases, Q_{MUT} presents longer paths than the other motions, indicating that besides the poorly connected interface residues, the interaction between TrkA monomers in mutant motions is weaker than in functional motions.

Residue E339 is located at TrkA DE loop and makes contact with N- and C-terminal regions of NGF subunits, that is, in the specific patch interface region. Suboptimal paths between E339 residues on both TrkA chains are shorter in Q_{NTR} motions than Q_{NCP} (Fig 9A). However, paths between residues H297 of each TrkA chain are shorter in Q_{NCP} motions than Q_{NTR} (Fig 9B). These residues are located in TrkA AB loop and also make contact with NGF specific patch residues, at NGF N-terminal region. TrkA residues Q350 that interacts with NGF conserved patch residues are linked by shorter paths in Q_{NTR} motions than in Q_{NCP} (Fig 9C). Also, paths between H297 and Q350 that connect both interface regions are shorter in Q_{NTR} motions than in Q_{NCP} (Fig 9D). These results show that Q_{NTR} and Q_{NCP} motions dynamically link TrkA interface residues differently, even those at the same interface region. Supplementary data of suboptimal path analysis of residues E334, M296, H298, and V354 are available in S1 Fig.

We evaluated the degeneracy of network nodes, which defines the percentage of the total paths crossing a given node, and observed that many of the most visited residues are also highly conserved in sequence, mainly in NGF (supplemental S4 Table). Interestingly, several residues with low conservation but high node degeneracy are residues that have been confirmed experimentally as crucial for binding and/or activation of TrkA signaling [17,50]. Moreover, we observed that residues F133 and H297 (NGF and TrkA chains, respectively) present a degeneracy close to the maximum in almost all paths calculated in Q_{MUT} motions, showing that the communication between TrkA chains is trapped in these nodes, thus avoiding information to flow through other paths.

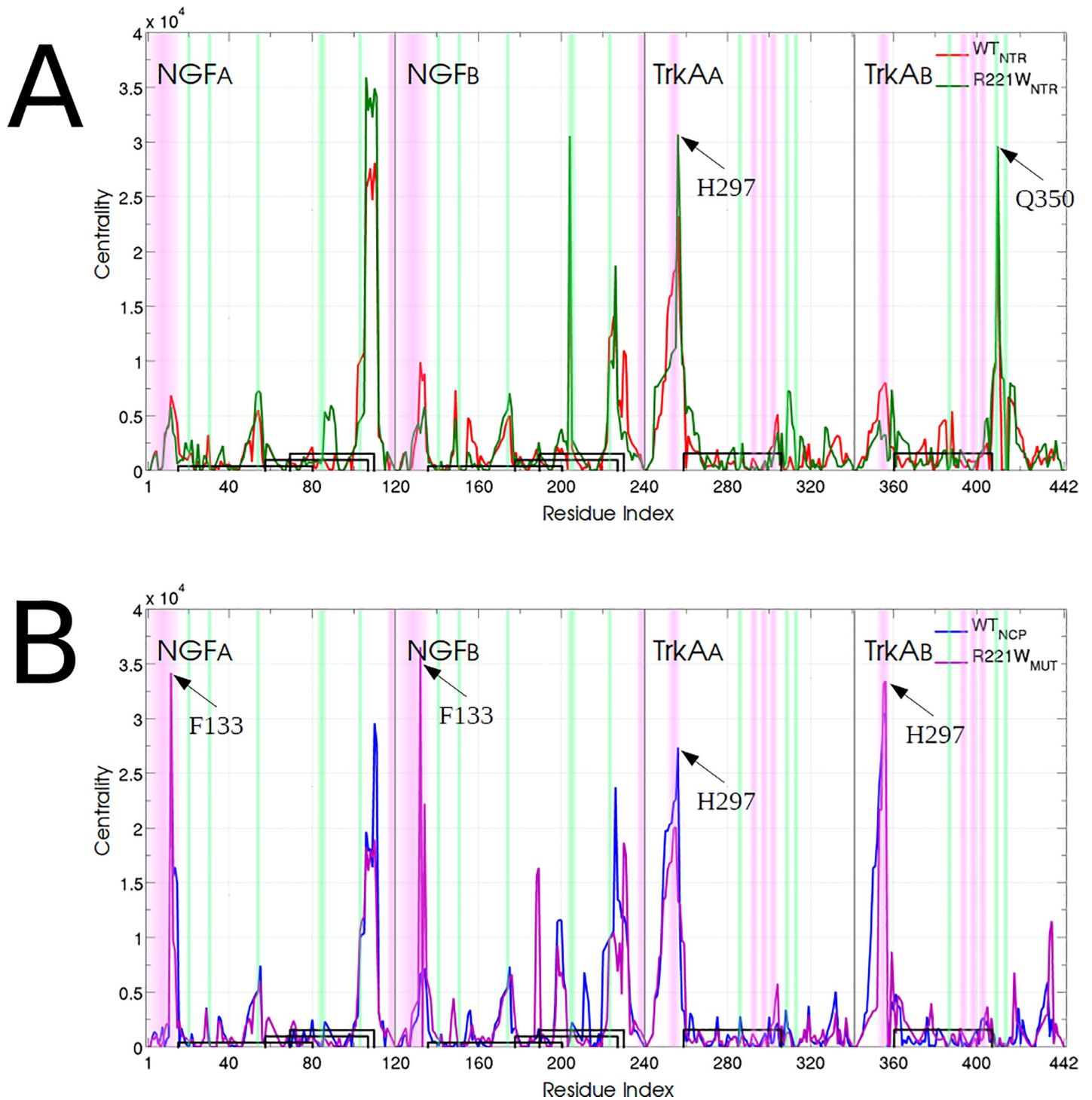


Fig 8. Differences in residue-wise centralities in dynamical networks. (A) Comparison between WT Q_{NTR} and R221W Q_{NTR} residue centralities indicates great similarity all along the complex. (B) Despite the similar centrality values for both TrkA chains, Q_{NCP} and Q_{MUT} present remarkable differences at NGF interface regions. Purple and green stripes indicate specificity and conserved patch residues, respectively. Arrows indicates residues with high degeneracy in interface regions. Black connectors represent disulfide bonds.

<https://doi.org/10.1371/journal.pone.0231542.g008>

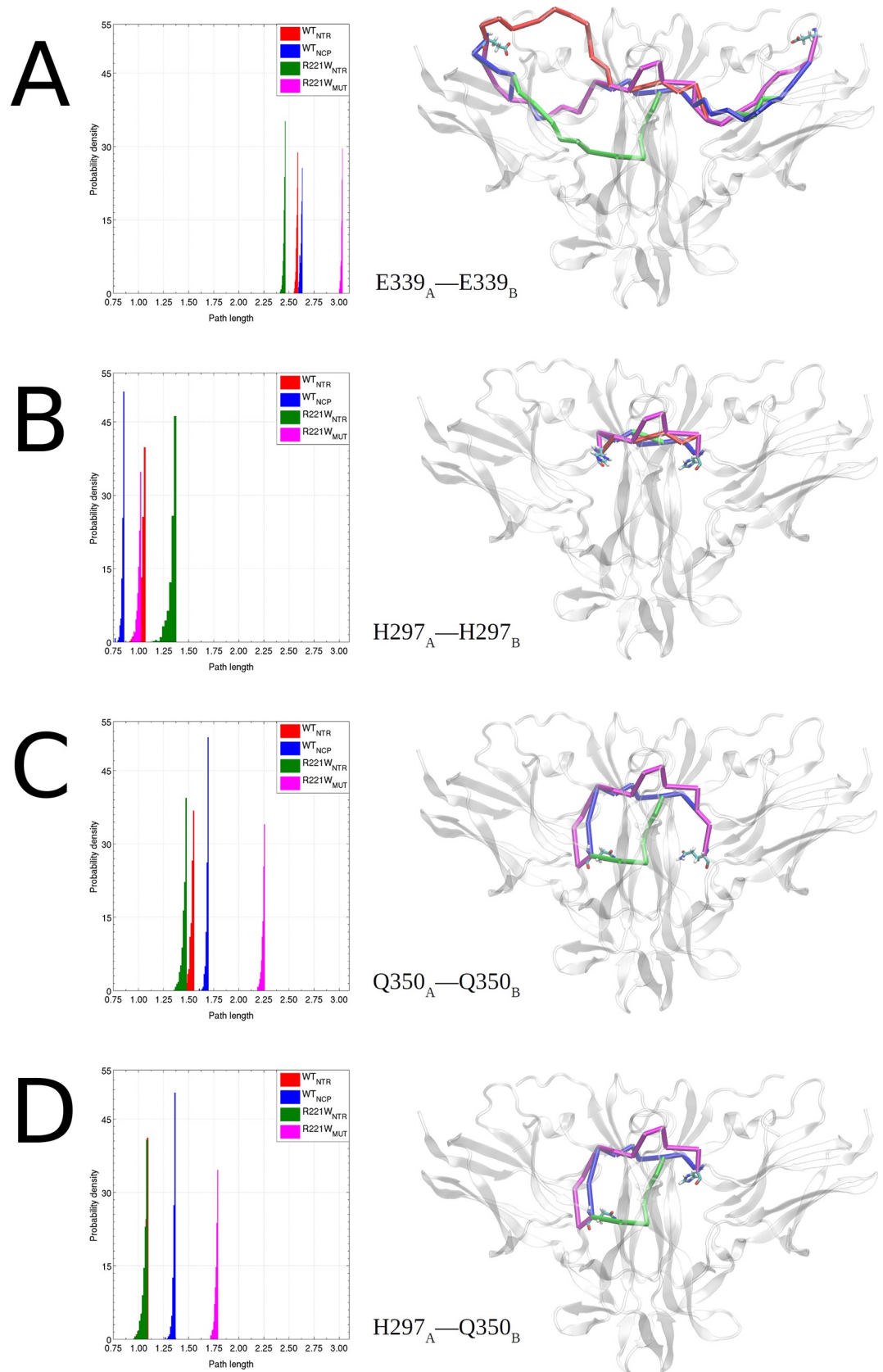


Fig 9. Optimal and suboptimal paths of interface residues. Optimal and suboptimal paths coupling the TrkA residues (A) E339_A–E339_B, (B) H297_A–H297_B, (C) Q350_A–Q350_B and (D) H297_A–Q350_B. Q_{NTR} motions can couple the two binding sites, while Q_{NCP} motions efficiently connect TrkA chains only via specific patch. The Q_{MUT} suboptimal paths are longer in almost all cases, which indicates its contribution to communication impairment. The shortest path is shown in the representation of the structure. Source and sink residues are presented as licorice. The histograms show the length distribution of the 500 paths calculated for each pair of residues.

<https://doi.org/10.1371/journal.pone.0231542.g009>

Discussion

In this study, we identified and analyzed the collective motions of the NGF/TrkA-Ig2 complex, related to the induction of each of the TrkA signaling outcomes (neurotrophic (Q_{NTR}) and nociception (Q_{NCP}) responses), and examined the structural and dynamical consequences of the NGF mutation R221W on inter-subunit interactions. We showed how this single mutation is capable of promoting drastic effects on NGF and the dynamics of TrkA, inhibiting the collective functional motions of the complex identified as responsible for inducing the activation of the nociceptive signaling of TrkA. To our knowledge, this is the very first study that reports on the inhibition of collective motions resulting from a single deleterious mutation in biased signaling processes. In addition, we showed that the R221W mutation also introduces novel collective motions into the system. We demonstrated that the removal of Q_{NTR} motion is linked to contact changes at NGF L1, L2, and L4 Loops. According to our results, Q_{NTR} motions (those shared by WT and R221W structures) can couple the two TrkA subunits through specific and conserved binding sites while Q_{NCP} motions (lost in R221W) couple TrkA monomers only through the specific binding site. Our data also shows the weakening of the dynamic coupling between the NGF and TrkA interface in the mutant specific motions (not appearing in WT), which was confirmed by network path calculations. The dynamical network analysis made it possible to identify the asymmetric coupling between TrkA-Ig2 domains in mutant motions. We highlighted several functionally essential residues for binding and/or specificity by performing network path analysis and comparing the most visited nodes with conserved residues in whole neurotrophin and Trk families. Moreover, we observed that suboptimal paths of Q_{MUT} motions are systematically longer than the other motions, indicating the impairment in the communication in these motions. Ultimately, we observed that atomic contacts and molecular interactions between residues involved in NGF binding and specificity were significantly changed by the mutation (see the [S1 Text](#)).

Collective motions have been widely demonstrated to be essential for protein function in many contexts [51–53]. The role of NGF in TrkA dimerization has been controversial for several years [13,26,54,55]. Besides whether receptor dimerization is induced or not by NGF binding, it is commonly accepted that only large scale conformational changes could activate TrkA signaling. Like other tyrosine kinase receptors, a rotational coupling of receptor monomers induced by the ligand would be required to receptor further signaling [56–58]. Since the Ig2 domain is responsible for NGF recognition [25,26], the putative activation dynamics comes from this interaction. This hypothesis was corroborated with our observation of rotational motions in the WT and R221W structures. However, these motions are not capable of fully induce the biased TrkA signaling, since the R221W mutation inhibits the PLC- γ 1 pathway [35], permanently impairing the nociceptive response [34,35,37,38]. Therefore, WT NGF presents a second mechanism to activate the nociception downstream promoted by TrkA, while R221W structures have this mechanism knocked-down as recently raised [59]. Here, we described the collective motions expected to be linked to the nociceptive response of the TrkA receptors and showed that the R221W complex is not capable reproducing these motions even when the WT motions were forced on the mutant structures.

Biased agonism has received much attention in recent years due to its relevance for understanding the signaling of several receptor types as well as for drug design [60–64]. The property to selectively activate one or other pathway is linked to the ligand's ability to induce the receptor to assume distinct conformations during the interaction [63]. This property is also often related to allostery [60,64,65]. We explored unusual dynamical characteristics of the complex by performing DCCM and dynamical network analysis. Despite the sharing of a common substructure community from each other, the motions presented particular connectivity, coupling the distal regions of the complex through different residues. The biased nature of TrkA receptors had already been studied [8]; however, how the NGF could lead to one or the other signaling outcome was still unclear. We presented how neurotrophic- and nociceptive-related motions change TrkA conformation by coupling specific and conserved patches distinctly. Q_{NTR} motions, common to WT and R221W complexes, link TrkA subunits through both interfaces, while Q_{NCP} motions efficiently couple TrkA through the specific patch alone.

Due to its neuroprotective action and its potential as a treatment for neurodegenerative and inflammatory conditions, neurotrophins have either been used themselves, as a treatment or mimicked in many studies over the past few years [66–70]. NGF therapeutic application is limited because of its poor plasma stability, inability to cross the blood-brain barrier, and the pleiotropic actions derived from its simultaneous connection to different receptors. Therefore, a strategy that has been approached is the construction of mutated structures [71] or small molecules that mimic its structure to act with both receptor or signaling specificity [8,67]. Our data helps to explain the molecular mechanisms involved in TrkA downstream activation mediated by WT and mutant NGF, providing new insights to novel development to trigger each signaling pathway specifically.

We presented an efficient approach based on normal mode analysis that effectively detects straightforwardly functional motions in a protein complex presenting multiple transduction signaling paths. The alternative using only standard molecular dynamics simulations would be extremely prohibitive and impractical since the observed functional movements are on the μ -ms time scale. Although principal components analysis (PCs) on shorter MD trajectories could capture the functional motions, they still remain very timely to carry out, with the caveat that the results are heavily dependent on the initial conditions and the MD simulation length. Our method presents also the advantage that the anharmonic aspects of the motions are taken into account through energy minimization and MD simulations when displacing the structures along the modes. There exists alternative Elastic Normal Modes (ENM) based methods that could be used for capturing the protein's global motions such as CoMD [72] but they only consider C α atoms in the first place, therefore one loses the direct effect of the mutated side chain on the mode direction which is essential in this study.

The only constraint of our approach is that it must first consider the experimental results on the effects of mutations on biased signaling to identify the associated functional motions. In this respect, it can be considered as an experimental-theoretical hybrid approach. Our method is more suitable for identifying large collective movements (linked to the function), but not local ones, although local interaction networks are taken into account in the collective movements by the NM analysis. Once the distinct functional motions are identified, a thorough study of the molecular and structural bases of the motions related to the signaling transduction path of interest lead to interesting insights. Drug specificity is often linked to the binding of a ligand to a particular region of the receptor. Since different motions activate different signaling pathways, the accessible sites exposed by the protein may vary allowing rational design of drugs binding to these sites. Consequently, the comparative identification of different set of functional motions makes it possible to understand the particular structural characteristics of each. The results of such an analysis can provide valuable tools in the area of drug design.

Methods

Molecular modeling and energy minimizations

The NGF/TrkA-Ig2 complex was built by considering the atomic coordinates from PDB entry 1WWW [15] which contains the homodimeric structure of NGF complexed with the homodimeric C-terminal immunoglobulin-like domain in a 2:2 stoichiometry. The few residue gaps in the structure were completed by using MODELLER 9.15 [73]. Co-crystallized water molecules were maintained in the final models. The lowest energy model was kept for further calculations. PyMOL 1.7 [74] was used to generate R221W mutant from the wild type model. Hydrogen atoms were added to the structure by PROPKA3 [75] observing a pH of 7.4.

Normal modes calculations and generation of low energy conformations along the normal modes vectors

Energy minimization and NM calculations were carried out using CHARMM c41b1 [76] and CHARMM force field parameter set 36 [77], with explicit TIP3P water molecules. Van der Waals interactions were calculated up to 10 Å, being approximated up to 12 Å using a switching function. Electrostatic interactions were calculated up to 10 Å. The WT and R221W structures were energy minimized using the steepest descent (SD) and CG methods followed by the Adopted-Basis Newton Raphson (ABNR) algorithm. Harmonic restraints were applied during 5×10^4 SD steps, being progressively decreased from 250 to 0 kcal/mol Å⁻². Then, the system was minimized with 10^6 steps of CG, and then with the ABNR algorithm without restraints using a convergence criterion of 10^{-5} kcal/mol Å⁻² RMS energy gradient. The 200 lowest normal modes for all atoms (excluding the 6 modes related to rigid body rotations and translations) were computed in vacuum using the DIMB [78] module implemented in CHARMM. A distance dependent dielectric constant ($\epsilon = 2r_{ij}$) was used to treat the electrostatic interactions. The NM and atomic fluctuations (root mean square fluctuations–RMSF) were computed with the VIBRAN module of CHARMM.

Relaxed conformations along the normal modes vectors were produced using the VMOD module in CHARMM as previously described [51]. It consists in carrying out a mass-weighted root mean square (MRMS) displacement of the structure along each normal mode through a successive molecular dynamics at low temperature (30 K) followed by energy minimizations. It uses restraining potentials for displacements along the normal mode coordinates and for freezing the overall translational and rotational motions added to the standard potential function, (see for more details in ref. [51]).

The generation of low energy structures along the modes is useful for taking into account anharmonic effects for large displacements, such as structural distortions, side chain rotations, formation or breaking of specific interactions, etc. This is not provided just by comparing directly the NM vectors. The generated structural trajectories, or structures generated at a given RMSD distance, can then be used for a more in-depth analysis to evaluate (dis)similarities when comparing different motions corresponding to normal modes.

Evaluation of similarity between distinct motions. Based on a previous study in Floquet et al., 2009 [51], the motions described by the lowest frequencies normal modes were characterized by establishing inter-atomic distance variation matrices over all the C α atoms for the displaced structures as explained in the previous chapter. For a given mode corresponding to a structure (WT or mutant), three matrices were considered: (i) the distance matrix corresponding to the X-ray energy minimized structure (M_{χ}) for which the modes were calculated; (ii) the distance matrix of the structure displaced at 1.0 Å of rmsd along the mode considered (M_{+}), and (iii) the matrix of the structure displaced at -1.0 Å (reversed direction) along the same

mode (M_-). The distance difference matrices equal to $(M_+ - M_x)$ or $(M_- - M_x)$, which represent the motions observed in the corresponding mode, were then evaluated. For the modes analyzed, as expected, it was observed that the M_+ and M_- matrices were highly related, thus only the $(M_+ - M_x)$ difference matrix was kept for analysis. The relative displacement matrices corresponding to all the modes considered were compared with one another by the Mantel correlation test, as implemented in the Vegan package version 2.3–1 [79] of R 3.2.3 software [80]. Using this method, we can assume that two matrices sharing a correlation coefficient equal to or greater than 0.6 ($p < 0.001$) describe closely related motions in 3D space [51].

Structural cross-correlation analysis

The structural correlations between the regions of the complex were calculated, taking into account the trajectories obtained along the individual normal modes as described above. The structural correlation between a pair of residues was calculated with the Eq 1:

$$C_{(ij)} = \frac{\langle \Delta r_i \cdot \Delta r_j \rangle}{\langle \Delta r_i^2 \rangle^{1/2} \cdot \langle \Delta r_j^2 \rangle^{1/2}} \quad (1)$$

where Δr_i is the coordinate displacement of atom i with respect to its average position in the structural trajectory; $\langle \dots \rangle$ means the average over all the structures. The covariance matrix is only established over the $C\alpha$ atoms. In this equation, the fully correlated motions (same phase and direction) have a value of +1 and the completely anti-correlated motions (same phase, different direction) have a value of -1. The calculations were performed in R 3.2.3 software using the Bio3D package version 2.3–1 [81].

Dynamical network analysis

In order to assess the effect of flexibility and structural changes on the structural communication between the NGF and TrkA subunits, a residue-residue coupling network was built using the correlation coefficients presented previously. We used a dynamical network method similar to that of Scarabelli et al. [45]. This network consists of an undirected weighted graph where each $C\alpha$ atom represents a node. Two nodes i and j were connected when their correlation value $|C_{(i,j)}| \geq 0.7$ and their $C\alpha$ - $C\alpha$ distance $d_{(i,j)} \leq 10\text{\AA}$ for at least 75% of total structures. The edges between nodes i and j were weighted ($w_{(i,j)}$) by their respective correlation value: $w_{(i,j)} = -\log(|C_{(i,j)}|)$. However, to avoid an unexpected partitioning created by the maximization of modularity, we applied a correction threshold (0.05 above maximum modularity). We reconstructed the network with partitions having modularity close to the maximum value but with a smaller overall number of communities. Also, communities under ten nodes were pruned. The hierarchical clustering was applied to aggregate highly correlated nodes into communities using the Girvan-Newman method [49]. A suboptimal path calculation was performed to identify the residues involved in the dynamic coupling of the binding sites. The calculations were performed with Bio3D package version 2.3–1.

Flexibility analysis

Flexibility was estimated as a root mean square average of $C\alpha$ atomic displacements over the set of structures of trajectories corresponding to a group of individual modes displaying similar motions with the Eq 2:

$$(rmsf)_s = \sqrt{\sum_{q=1}^{n_s} \frac{1}{n_s} \frac{1}{3N} \sum_{i=1}^{3N} (r_{qi} - r_{qi}^0)^2} \quad (2)$$

where s indexes a group of similar normal modes, n_s is the number of modes in this group, N the number of atoms considered, r_{qi} the coordinate of the atom corresponding to the degree of freedom i and the mode number q , and r_{qi}^0 to that of the initial structure.

Hydrogen bonds and salt bridges analyses

Hydrogen bond (hbond) and salt bridge formation were analyzed using VMD 1.9.2 plugins [82]. The hbond donor-acceptor distance was set to 3.0 Å, and the cutoff angle was set to 20°. The oxygen-nitrogen distance was set at 3.2 Å for the analysis the salt bridges. High occupancy interactions was set to a minimum of 50% in the trajectory of each type of motion [83]. To confirm the hbond changes, we analyzed the structures using the Baker & Hubbard criteria with MDTraj 1.2 software [84].

Graphical representations

Graphical views of the models were performed with VMD 1.9.2 and PyMOL 1.7.

Supporting information

S1 Text. Local topological changes lead to long range structural effects.

(DOCX)

S1 Fig. Optimal and suboptimal paths of interface residues. Optimal and suboptimal paths coupling TrkA residues (A) E334_A–E334_B, (B) M296_A–M296_B, (C) H298_A–H298_B, and (D) V354_A–V354_B. The shortest path is shown in structure representation. Source and sink residues are presented as licorice. Histograms show the length distribution of the 500 paths calculated for each residue pair.

(TIFF)

S2 Fig. Contact map changes at position 221. All atom contact changes in a radius of 10 Å of position 221 of both (A) NGF_A and (B) NGF_B. (C) Structural representation of residues with contacts changes. Red and blue spheres indicate residues with contacts lost and acquired in R221W mutant with respect to WT, respectively. Chains are colored as: NGF_A: green; NGF_B: cyan; TrkA_A: magenta; TrkA_B: yellow. Residues R221 are represented as orange sticks.

(TIFF)

S3 Fig. Flexibility changes in WT and R221W motions. Cα root-mean-squared fluctuation (A) WT Q_{NTR} , (B) R221W Q_{NTR} , (C) Q_{NCP} and (D) Q_{MUT} . Purple and green stripes indicate specificity and conserved patch residues, respectively. Black connectors represent disulfide bonds.

(TIFF)

S4 Fig. Residues involved in significant hydrogen bond changes in WT and R221W motions. Red and blue sticks represent presence or absence of interactions, respectively, in (A) Q_{NCP} motions and (B) Q_{MUT} motions. Residues colored in gray are present in both (A) WT motions or (B) R221W motions. Chains are colored as: NGF_A: green; NGF_B: cyan; TrkA_A: magenta; TrkA_B: yellow. Black spheres indicates interacting residues that are also involved in binding and specificity.

(TIFF)

S1 Table. Correlation among the 20 lowest frequency normal modes of WT and R221W complexes. Correlated modes are shown in gold cells with values in bold. Only modes with

correlation coefficient $\geq |0.6|$ were highlighted (except the diagonal).
(XLS)

S2 Table. Correlation among WT and R221W structures displaced along NCP motions.

Correlated modes are shown in gold cells with values in bold. Only modes with correlation coefficient $\geq |0.6|$ were highlighted.

(XLS)

S3 Table. Correlation among the 20 lowest frequency normal modes of wild type complex and several mutant structures.

Correlated modes are shown in gold cells with values in bold.

Only modes with correlation coefficient $\geq |0.6|$ were highlighted.

(XLS)

S4 Table. Node degeneracy from optimal path analysis of correlation networks. For each network, 500 suboptimal paths were calculated. Nodes with degeneracy ≥ 0.1 in one or more networks are shown and corresponding degeneracy values are colored in red, green, blue and magenta, respectively, for WT Q_{NTR} , R221W Q_{NTR} , Q_{NCP} and Q_{MUT} networks. Source and sink nodes are highlighted in light gray. Residues identified as binding determinants are shown in bold.

(XLS)

Author Contributions

Conceptualization: Pedro Túlio Resende-Lara, David Perahia, Ana Lgia Scott, Antnio Srgio Kimus Braz.

Data curation: Pedro Túlio Resende-Lara.

Formal analysis: Pedro Túlio Resende-Lara.

Investigation: Pedro Túlio Resende-Lara.

Methodology: Pedro Túlio Resende-Lara, David Perahia, Ana Lgia Scott, Antnio Srgio Kimus Braz.

Resources: Pedro Túlio Resende-Lara, David Perahia, Ana Lgia Scott, Antnio Srgio Kimus Braz.

Supervision: David Perahia, Antnio Srgio Kimus Braz.

Validation: Pedro Túlio Resende-Lara, David Perahia, Ana Lgia Scott.

Visualization: Pedro Túlio Resende-Lara.

Writing – original draft: Pedro Túlio Resende-Lara.

Writing – review & editing: Pedro Túlio Resende-Lara, David Perahia, Ana Lgia Scott, Antnio Srgio Kimus Braz.

References

1. Benovic JL, Strasser RH, Caron MG, Lefkowitz RJ. Beta-adrenergic receptor kinase: identification of a novel protein kinase that phosphorylates the agonist-occupied form of the receptor. *Proc Natl Acad Sci*. 1986; 83: 2797–2801. <https://doi.org/10.1073/pnas.83.9.2797> PMID: 2871555
2. Rasmussen SGF, Devree BT, Zou Y, Kruse AC, Chung KY, Kobilka TS, et al. Crystal structure of the β 2adrenergic receptor-Gs protein complex. *Nature*. 2011; 477: 549–557. <https://doi.org/10.1038/nature10361> PMID: 21772288

3. Liu JJ, Horst R, Katritch V, Stevens RC, Wüthrich K. Biased signaling pathways in β 2-adrenergic receptor characterized by 19F-NMR. *Science*. 2012; 335: 1106–10. <https://doi.org/10.1126/science.1215802> PMID: 22267580
4. Fribourg M, Moreno JL, Holloway T, Provasi D, Baki L, Mahajan R, et al. Decoding the Signaling of a GPCR Heteromeric Complex Reveals a Unifying Mechanism of Action of Antipsychotic Drugs. *Cell*. 2011; 147: 1011–1023. <https://doi.org/10.1016/j.cell.2011.09.055> PMID: 22118459
5. Thompson GL, Lane JR, Coudrat T, Sexton PM, Christopoulos A, Canals M. Biased Agonism of Endogenous Opioid Peptides at the μ -Opioid Receptor. *Mol Pharmacol*. 2015; 88: 335–346. <https://doi.org/10.1124/mol.115.098848> PMID: 26013541
6. Khajehali E, Malone DT, Glass M, Sexton PM, Christopoulos A, Leach K. Biased Agonism and Biased Allosteric Modulation at the CB1 Cannabinoid Receptor. *Mol Pharmacol*. 2015; 88: 368–79. <https://doi.org/10.1124/mol.115.099192> PMID: 26044547
7. Sengmany K, Singh J, Stewart GD, Conn PJ, Christopoulos A, Gregory KJ. Biased allosteric agonism and modulation of metabotropic glutamate receptor 5: Implications for optimizing preclinical neuroscience drug discovery. *Neuropharmacology*. 2017; 115: 60–72. <https://doi.org/10.1016/j.neuropharm.2016.07.001> PMID: 27392634
8. Brahimi F, Ko E, Malakhov A, Burgess K, Saragovi HU. Combinatorial assembly of small molecules into bivalent antagonists of TrkC or TrkA receptors. *PLoS One*. 2014; 9: e89617. <https://doi.org/10.1371/journal.pone.0089617> PMID: 24603864
9. Freed DM, Bessman NJ, Kiyatkin A, Salazar-Cavazos E, Byrne PO, Moore JO, et al. EGFR Ligands Differentially Stabilize Receptor Dimers to Specify Signaling Kinetics. *Cell*. 2017; 171: 683–695.e18. <https://doi.org/10.1016/j.cell.2017.09.017> PMID: 28988771
10. Henzler-Wildman K, Kern D. Dynamic personalities of proteins. *Nature*. 2007; 450: 964–972. <https://doi.org/10.1038/nature06522> PMID: 18075575
11. Tsai C-J, Kumar S, Ma B, Nussinov R. Folding funnels, binding funnels, and protein function. *Protein Sci*. 1999; 8: 1181–1190. <https://doi.org/10.1110/ps.8.6.1181> PMID: 10386868
12. Tsai C-J, Kumar S, Ma B, Nussinov R. Folding funnels and binding mechanisms. *Protein Sci*. 1999; 8: 1181–1190. <https://doi.org/10.1110/ps.8.6.1181> PMID: 10386868
13. Shen J, Maruyama IN. Nerve growth factor receptor TrkA exists as a preformed, yet inactive, dimer in living cells. *FEBS Lett*. 2011; 585: 295–299. <https://doi.org/10.1016/j.febslet.2010.12.031> PMID: 21187090
14. Reichardt LF. Neurotrophin-regulated signalling pathways. *Philos Trans R Soc Lond B Biol Sci*. 2006; 361: 1545–64. <https://doi.org/10.1098/rstb.2006.1894> PMID: 16939974
15. Wiesmann C, Ultsch MH, Bass SH, de Vos AM. Crystal structure of nerve growth factor in complex with the ligand-binding domain of the TrkA receptor. *Nature*. 1999; 401: 184–8. <https://doi.org/10.1038/43705> PMID: 10490030
16. Urfer R, Tsoulfas P, O'Connell L, Hongo J-A, Zhao W, Presta LG. High Resolution Mapping of the Binding Site of TrkA for Nerve Growth Factor and TrkC for Neurotrophin-3 on the Second Immunoglobulin-like Domain of the Trk Receptors. *J Biol Chem*. 1998; 273: 5829–5840. <https://doi.org/10.1074/jbc.273.10.5829> PMID: 9488719
17. O'Connell L, Hongo JA, Presta LG, Tsoulfas P. TrkA amino acids controlling specificity for nerve growth factor. *J Biol Chem*. 2000; 275: 7870–7877. <https://doi.org/10.1074/jbc.275.11.7870> PMID: 10713102
18. Shih A, Laramée GR, Schmelzer CH, Burton LE, Winslow JW. Mutagenesis identifies amino-terminal residues of nerve growth factor necessary for Trk receptor binding and biological activity. *J Biol Chem*. 1994; 269: 27679–86. Available: <http://www.jbc.org/content/269/44/27679.abstract> PMID: 7961687
19. Kruttgen A, Heymach J V., Kahle PJ, Shooter EM. The Role of the Nerve Growth Factor Carboxyl Terminus in Receptor Binding and Conformational Stability. *J Biol Chem*. 1997; 272: 29222–29228. <https://doi.org/10.1074/jbc.272.46.29222> PMID: 9361001
20. Guo M, Meyer SL, Kaur H, Gao JJ, Neet KE. Mutational studies of conserved residues in the dimer interface of nerve growth factor. *Protein Sci*. 1996; 5: 447–55. <https://doi.org/10.1002/pro.5560050306> PMID: 8868481
21. Ibáñez CF, Lilag L, Murray-Rust J1, Persson H. An extended surface of binding to Trk tyrosine kinase receptors in NGF and BDNF allows the engineering of a multifunctional pan-neurotrophin. *EMBO J*. 1993; 12: 2281–2293. Available: <https://www.ncbi.nlm.nih.gov/pmc/articles/PMC413458/pdf/emboj00078-0059.pdf> PMID: 8508763
22. Drinkwater CC, Barker PA, Suter U, Shooter EM. The carboxyl terminus of nerve growth factor is required for biological activity. *J Biol Chem*. 1993; 268: 23202–23207. Available: http://www.ncbi.nlm.nih.gov/entrez/query.fcgi?cmd=Retrieve&db=PubMed&dopt=Citation&list_uids=8226840 PMID: 8226840

23. Ibáñez CF, Ebendal T, Barbany G, Murray-Rust J, Blundell TL, Persson H. Disruption of the low affinity receptor-binding site in NGF allows neuronal survival and differentiation by binding to the *trk* gene product. *Cell*. 1992; 69: 329–341. [https://doi.org/10.1016/0092-8674\(92\)90413-7](https://doi.org/10.1016/0092-8674(92)90413-7) PMID: 1314703
24. Ibáñez CF, Hallböök F, Ebendal T, Persson H. Structure-function studies of nerve growth factor: functional importance of highly conserved amino acid residues. *EMBO J*. 1990; 9: 1477–83. PMID: 2328722
25. Urferl R, Tsoulfas P2, O'connell L, Shelton DL4, Parada LF2, Presta LG. An immunoglobulin-like domain determines the specificity of neurotrophin receptors. *EMBO J*. 1995; 14: 2795–2805. Available: <https://www.ncbi.nlm.nih.gov/pmc/articles/PMC398398/pdf/emboj00036-0117.pdf> PMID: 7796806
26. Arevalo JC, Conde B, Hempstead BL, Chao M V, Martín-Zanca D, Pérez P. TrkA immunoglobulin-like ligand binding domains inhibit spontaneous activation of the receptor. *Mol Cell Biol*. 2000; 20: 5908–5916. <https://doi.org/10.1128/mcb.20.16.5908-5916.2000> PMID: 10913174
27. Arevalo JC, Conde B, Hempstead BI, Chao M V, Martín-Zanca D, Pérez P. A novel mutation within the extracellular domain of TrkA causes constitutive receptor activation. *Oncogene*. 2001; 20: 1229–1234. <https://doi.org/10.1038/sj.onc.1204215> PMID: 11313867
28. Latz E, Verma A, Visintin A, Gong M, Sirois CM, Klein DCG, et al. Ligand-induced conformational changes allosterically activate Toll-like receptor 9. *Nat Immunol*. 2007; 8: 772–9. <https://doi.org/10.1038/ni1479> PMID: 17572678
29. Livnah O, Johnson DL, Stura EA, Farrell FX, Barbone FP, You Y, et al. An antagonist peptide-EPO receptor complex suggests that receptor dimerization is not sufficient for activation. *Nat Struct Biol*. 1998; 5: 993–1004. <https://doi.org/10.1038/2965> PMID: 9808045
30. Moriki T, Maruyama H, Maruyama IN. Activation of preformed EGF receptor dimers by ligand-induced rotation of the transmembrane domain. *J Mol Biol*. 2001; 311: 1011–26. <https://doi.org/10.1006/jmbi.2001.4923> PMID: 11531336
31. Tao R-H, Maruyama IN. All EGF(ErbB) receptors have preformed homo- and heterodimeric structures in living cells. *J Cell Sci*. 2008; 121: 3207–17. <https://doi.org/10.1242/jcs.033399> PMID: 18782861
32. Marlin MC, Li G. Biogenesis and Function of the NGF/TrkA Signaling Endosome. *International Review of Cell and Molecular Biology*. 2015. pp. 239–257. <https://doi.org/10.1016/bs.ircmb.2014.10.002> PMID: 25619719
33. Carvalho OP, Thornton GK, Hertecant J, Houlden H, Nicholas AK, Cox JJ, et al. A novel NGF mutation clarifies the molecular mechanism and extends the phenotypic spectrum of the HSAN5 neuropathy. *J Med Genet*. 2011; 48: 131–135. <https://doi.org/10.1136/jmg.2010.081455> PMID: 20978020
34. Capsoni S. From genes to pain: nerve growth factor and hereditary sensory and autonomic neuropathy type V. *Eur J Neurosci*. 2014; 39: 392–400. <https://doi.org/10.1111/ejn.12461> PMID: 24494679
35. Capsoni S, Covaceuszach S, Marinelli S, Ceci M, Bernardo A, Minghetti L, et al. Taking pain out of NGF: a “painless” NGF mutant, linked to hereditary sensory autonomic neuropathy type V, with full neurotrophic activity. *PLoS One*. 2011; 6: e17321. <https://doi.org/10.1371/journal.pone.0017321> PMID: 21387003
36. Einarsdottir E, Carlsson A, Minde J, Toolanen G, Svensson O, Solders G, et al. A mutation in the nerve growth factor beta gene (NGFB) causes loss of pain perception. *Hum Mol Genet*. 2004; 13: 799–805. <https://doi.org/10.1093/hmg/ddh096> PMID: 14976160
37. Larsson E, Kuma R, Norberg A, Minde J, Holmberg M. Nerve growth factor R221W responsible for insensitivity to pain is defectively processed and accumulates as proNGF. *Neurobiol Dis*. 2009; 33: 221–228. <https://doi.org/10.1016/j.nbd.2008.10.012> PMID: 19038341
38. Covaceuszach S, Capsoni S, Marinelli S, Pavone F, Ceci M, Ugolini G, et al. In vitro receptor binding properties of a “painless” NGF mutein, linked to hereditary sensory autonomic neuropathy type V. *Biochem Biophys Res Commun*. 2010. <https://doi.org/10.1016/j.bbrc.2009.11.146> PMID: 19945432
39. Settanni G, Cattaneo A, Carloni P. Molecular dynamics simulations of the NGF-TrkA domain 5 complex and comparison with biological data. *Biophys J*. 2003; 84: 2282–92. [https://doi.org/10.1016/S0006-3495\(03\)75034-6](https://doi.org/10.1016/S0006-3495(03)75034-6) PMID: 12668437
40. Houlden H, King RHM, Hashemi-Nejad A, Wood NW, Mathias CJ, Reilly M, et al. A novel TRK A (NTRK1) mutation associated with hereditary sensory and autonomic neuropathy type V. *Ann Neurol*. 2001; 49: 521–525. <https://doi.org/10.1002/ana.103.abs> PMID: 11310631
41. Guarnera E, Berezovsky IN. Allosteric sites: Remote control in regulation of protein activity. *Current Opinion in Structural Biology*. 2016. pp. 1–8. <https://doi.org/10.1016/j.sbi.2015.10.004> PMID: 26562539
42. Stolzenberg S, Michino M, Levine M V., Weinstein H, Shi L. Computational approaches to detect allosteric pathways in transmembrane molecular machines. *Biochim Biophys Acta—Biomembr*. 2016; 1858: 1652–1662. <https://doi.org/10.1016/j.bbamem.2016.01.010> PMID: 26806157

43. Gasper PM, Fuglestad B, Komives EA, Markwick PRL, McCammon JA. Allosteric networks in thrombin distinguish procoagulant vs. anticoagulant activities. *Proc Natl Acad Sci U S A*. 2012; 109: 21216–22. <https://doi.org/10.1073/pnas.1218414109> PMID: 23197839
44. Scarpi D, Cirelli D, Matrone C, Castronovo G, Rosini P, Occhiato EG, et al. Low molecular weight, non-peptidic agonists of TrkA receptor with NGF-mimetic activity. *Cell Death Dis*. 2012; 3: e339. <https://doi.org/10.1038/cddis.2012.80> PMID: 22764098
45. Scarabelli G, Grant BJ. Kinesin-5 allosteric inhibitors uncouple the dynamics of nucleotide, microtubule, and neck-linker binding sites. *Biophys J*. 2014; 107: 2204–13. <https://doi.org/10.1016/j.bpj.2014.09.019> PMID: 25418105
46. Sethi A, Eargle J, Black AA, Luthey-Schulten Z. Dynamical networks in tRNA:protein complexes. *Proc Natl Acad Sci U S A*. 2009; 106: 6620–5. <https://doi.org/10.1073/pnas.0810961106> PMID: 19351898
47. Van Wart AT, Durrant J, Votapka L, Amaro RE. Weighted Implementation of Suboptimal Paths (WISP): An Optimized Algorithm and Tool for Dynamical Network Analysis. *J Chem Theory Comput*. 2014; 10: 511–517. <https://doi.org/10.1021/ct4008603> PMID: 24803851
48. Yao X-Q, Skjærven L, Grant BJ. Rapid Characterization of Allosteric Networks with Ensemble Normal Mode Analysis. *J Phys Chem B*. 2016; 120: In press. <https://doi.org/10.1021/acs.jpcc.6b01991> PMID: 27056373
49. Girvan M, Newman MEJ. Community structure in social and biological networks. *Proc Natl Acad Sci U S A*. 2002; 99: 7821–6. <https://doi.org/10.1073/pnas.122653799> PMID: 12060727
50. Pattarawarapan M, Burgess K. Molecular Basis of Neurotrophin–Receptor Interactions. *J Med Chemistry*. 2003; 46: 5277–5291. <https://doi.org/10.1021/jm030221q> PMID: 14640536
51. Floquet N, Durand P, Maigret B, Badet B, Badet-Denisot M-A, Perahia D. Collective motions in glucosamine-6-phosphate synthase: influence of ligand binding and role in ammonia channelling and opening of the fructose-6-phosphate binding site. *J Mol Biol*. 2009; 385: 653–64. <https://doi.org/10.1016/j.jmb.2008.10.032> PMID: 18976669
52. Costa MGS, Batista PR, Bisch PM, Perahia D. Exploring Free Energy Landscapes of Large Conformational Changes: Molecular Dynamics with Excited Normal Modes. *J Chem Theory Comput*. 2015; 11: 2755–2767. <https://doi.org/10.1021/acs.jctc.5b00003> PMID: 26575568
53. Yao X-QQ, Malik RU, Griggs NW, Skjærven L, Traynor JR, Sivaramakrishnan S, et al. Dynamic coupling and allosteric networks in the α subunit of heterotrimeric G proteins. *J Biol Chem*. 2016; 291: 4742–4753. <https://doi.org/10.1074/jbc.M115.702605> PMID: 26703464
54. Mischel PS, Umbach J a, Eskandari S, Smith SG, Gundersen CB, Zampighi G a. Nerve growth factor signals via preexisting TrkA receptor oligomers. *Biophys J*. 2002; 83: 968–976. [https://doi.org/10.1016/S0006-3495\(02\)75222-3](https://doi.org/10.1016/S0006-3495(02)75222-3) PMID: 12124278
55. Mehta HM, Woo SB, Neet KE. Comparison of nerve growth factor receptor binding models using heterodimeric muteins. *J Neurosci Res*. 2012; 90: 2259–2271. <https://doi.org/10.1002/jnr.23116> PMID: 22903500
56. Gong Y, Cao P, Yu H, Jiang T. Crystal structure of the neurotrophin-3 and p75NTR symmetrical complex. *Nature*. 2008; 454: 789–93. <https://doi.org/10.1038/nature07089> PMID: 18596692
57. Maruyama IN. Mechanisms of Activation of Receptor Tyrosine Kinases: Monomers or Dimers. *Cells*. 2014; 3: 304–330. <https://doi.org/10.3390/cells3020304> PMID: 24758840
58. Bradshaw RA, Chalkley RJ, Biarc J, Burlingame AL. Receptor tyrosine kinase signaling mechanisms: Devolving TrkA responses with phosphoproteomics. *Adv Biol Regul*. 2013; 53: 87–96. <https://doi.org/10.1016/j.jbior.2012.10.006> PMID: 23266087
59. Sung K, Ferrari LF, Yang W, Chung C, Zhao X, Gu Y, et al. Swedish Nerve Growth Factor Mutation (NGFR100W) Defines a Role for TrkA and p75NTR in Nociception. *J Neurosci*. 2018; 1686–17. <https://doi.org/10.1523/JNEUROSCI.1686-17.2018> PMID: 29483280
60. Ehler FJ. Functional studies cast light on receptor states. *Trends Pharmacol Sci*. 2015; 1–9. <https://doi.org/10.1016/j.tips.2015.05.008> PMID: 26123416
61. Ikeda Y, Kumagai H, Motozawa Y, Suzuki J-I, Komuro I. Biased Agonism of the Angiotensin II Type I Receptor. *Int Heart J*. 2015; 56: 485–488. <https://doi.org/10.1536/ihj.15-256> PMID: 26180022
62. Griffin JH, Zlokovic BV, Mosnier LO. Activated protein C: biased for translation. *Blood*. 2015; 125: 2898–907. <https://doi.org/10.1182/blood-2015-02-355974> PMID: 25824691
63. Rankovic Z, Brust TF, Bohn LM. Biased agonism: An emerging paradigm in GPCR drug discovery. *Bioorg Med Chem Lett*. 2015; 26: 241–250. <https://doi.org/10.1016/j.bmcl.2015.12.024> PMID: 26707396
64. Leach K, Conigrave AD, Sexton PM, Christopoulos A. Towards tissue-specific pharmacology: insights from the calcium-sensing receptor as a paradigm for GPCR (patho)physiological bias. *Trends Pharmacol Sci*. 2015; 36: 215–25. <https://doi.org/10.1016/j.tips.2015.02.004> PMID: 25765207

65. Wisler JW, Xiao K, Thomsen ARB, Lefkowitz RJ. Recent developments in biased agonism. *Curr Opin Cell Biol.* 2014; 27: 18–24. <https://doi.org/10.1016/j.ceb.2013.10.008> PMID: 24680426
66. Longo FM, Xie Y, Massa SM. Neurotrophin Small Molecule Mimetics: Candidate Therapeutic Agents for Neurological Disorders. *Curr Med Chem.* 2005; 5: 29–41.
67. Longo FM, Massa SM. Small-molecule modulation of neurotrophin receptors: a strategy for the treatment of neurological disease. *Nat Rev Drug Discov.* 2013; 12: 507–525. <https://doi.org/10.1038/nrd4024> PMID: 23977697
68. Mantyh PW, Koltzenburg M, Mendell LM, Tive L, Shelton DL. Antagonism of Nerve Growth Factor-TrkA Signaling and the Relief of Pain. *Anesthesiology.* 2011; 115: 189–204. <https://doi.org/10.1097/ALN.0b013e31821b1ac5> PMID: 21602663
69. Zhang Q, Descamps O, Hart MJ, Poksay KS, Spilman P, Kane DJ, et al. Paradoxical effect of TrkA inhibition in alzheimer's disease models. *J Alzheimer's Dis.* 2014; 40: 605–617. <https://doi.org/10.3233/JAD-130017> PMID: 24531152
70. Rizzi C, Tiberi A, Giustizieri M, Marrone MC, Gobbo F, Carucci NM, et al. NGF steers microglia toward a neuroprotective phenotype. *Glia.* 2018 [cited 6 Mar 2018]. <https://doi.org/10.1002/glia.23312> PMID: 29473218
71. Carleton LA, Chakravarthy R, van der Sloot AM, Mnich K, Serrano L, Samali A, et al. Generation of rationally-designed nerve growth factor (NGF) variants with receptor specificity. *Biochem Biophys Res Commun.* 2018; 495: 700–705. <https://doi.org/10.1016/j.bbrc.2017.11.003> PMID: 29108999
72. Gur M, Madura JD, Bahar I. Global transitions of proteins explored by a multiscale hybrid methodology: Application to adenylate kinase. *Biophys J.* 2013; 105: 1643–1652. <https://doi.org/10.1016/j.bpj.2013.07.058> PMID: 24094405
73. Webb B, Sali A. Comparative Protein Structure Modeling Using Modeller. *Current Protocols in Bioinformatics.* 2016. pp. 5.6.1–5.6.37. <https://doi.org/10.1002/cpbi.3> PMID: 27322406
74. Schrödinger L. The PyMOL Molecular Graphics System, Version~1.8. 2015.
75. Olsson MHM, Søndergaard CR, Rostkowski M, Jensen JH. PROPKA3: Consistent Treatment of Internal and Surface Residues in Empirical pKa Predictions. *J Chem Theory Comput.* 2011; 7: 525–537. <https://doi.org/10.1021/ct100578z> PMID: 26596171
76. Brooks BRR, Brooks CLL, MacKerell ADD Jr., Nilsson L, Petrella RJJ, Roux B, et al. CHARMM: The Biomolecular Simulation Program. *J Comput Chem.* 2010; 30: 1545–1614. <https://doi.org/10.1002/jcc.21287>. CHARMM
77. Huang J, Mackerell AD. CHARMM36 all-atom additive protein force field: Validation based on comparison to NMR data. *J Comput Chem.* 2013; 34: 2135–2145. <https://doi.org/10.1002/jcc.23354> PMID: 23832629
78. Perahia D, Mouawad L. Computation of low-frequency normal modes in macromolecules: improvements to the method of diagonalization in a mixed basis and application to hemoglobin. *Comput Chem.* 1995; 19: 241–246. [https://doi.org/10.1016/0097-8485\(95\)00011-g](https://doi.org/10.1016/0097-8485(95)00011-g) PMID: 7551557
79. Oksanen J, Blanchet FG, Kindt R, Legendre P, Minchin PR, O'Hara RB, et al. vegan: Community Ecology Package. R package version 2.2–1. 2015. Available: <http://cran.r-project.org/package=vegan>
80. R Core Team. R: A language and environment for statistical computing. R Foundation for Statistical Computing. Vienna; 2016. Available: <http://www.r-project.org/>
81. Grant BJ, Rodrigues APC, ElSawy KM, McCammon JA, Caves LSD. Bio3d: an R package for the comparative analysis of protein structures. *Bioinformatics.* 2006; 22: 2695–2696. <https://doi.org/10.1093/bioinformatics/btl461> PMID: 16940322
82. Humphrey W, Dalke A, Schulten K. VMD: visual molecular dynamics. *J Mol Graph.* 1996; 14: 27–28,33–38. Available: <http://www.ncbi.nlm.nih.gov/pubmed/8744570>
83. Reyes CM, Nifosi R, Frankel a D, Kollman P a. Molecular dynamics and binding specificity analysis of the bovine immunodeficiency virus BIV Tat-TAR complex. *Biophys J.* 2001; 80: 2833–42. [https://doi.org/10.1016/S0006-3495\(01\)76250-9](https://doi.org/10.1016/S0006-3495(01)76250-9) PMID: 11371457
84. McGibbon RT, Beauchamp KA, Harrigan MP, Klein C, Swails JM, Hernández CX, et al. MDTraj: A Modern Open Library for the Analysis of Molecular Dynamics Trajectories. *Biophys J.* 2015; 109: 1528–1532. <https://doi.org/10.1016/j.bpj.2015.08.015> PMID: 26488642